Water Supply

IWA PUBLISHING

Water Supply Vol 23 No 11, 4592 doi: 10.2166/ws.2023.283

Assessment of drought variability in the Marrakech-Safi region (Morocco) at different time scales using GIS and remote sensing

Chaima Elair [a,*], Khalid Rkha Chaham[a] and Abdessamad Hadri[b]

[a] DLGR Laboratory, Department of Geology, Faculty of Sciences Semlalia, Cadi Ayyad University, Marrakech 40000, Morocco
[b] International Water Research Institute (IWRI), Mohammed VI Polytechnic University (UM6P), Benguerir 43150, Morocco
*Corresponding author. E-mail: elairchaima@gmail.com

CE, 0000-0001-8084-9837

ABSTRACT

In the semi-arid Marrakech-Safi (MS) region of southwest Morocco, climate change has amplified drought occurrences, posing significant threats to water resources and agriculture. A comprehensive understanding of drought patterns is imperative to manage these risks and enhance resilience effectively. Precipitation from 18 pluviometer stations was employed to analyze meteorological drought using the standardized precipitation index (SPI) from 1980 to 2018. Additionally, agricultural drought is quantified using three remote sensing-driven indices: vegetation condition index (VCI), temperature conditions index (TCI), and vegetation health index (VHI) from 2000 to 2018. These indices are correlated with SPI to evaluate their performance and gauge vegetation sensitivity to meteorological drought. The Mann–Kendall test assesses trends in drought events and their severity. The results demonstrated that SPI, VCI, TCI, and VHI experienced alternating dry and wet periods with an overall upward trend, especially in mountainous areas, plateau zones, and Haouz plain of the MS region. The correlation analysis establishes a significant relationship between remote sensing-based indices and SPI-6, with mean correlation coefficients exceeding 0.6. The findings underscore the importance of considering multiple time scales to comprehensively assess climate's impact on vegetation. Seasonal drought trends analysis indicates no significant negative trends in winter and spring but positive trends in autumn.

Key words: drought, geographic information system (GIS), remote sensing, SPI, VCI, VHI

HIGHLIGHTS

- Use the SPI to study meteorological droughts between 1980 and 2018.
- Use Mann–Kendall and Sen's slope estimators to analyze seasonal and yearly SPI trends.
- Spatio-temporal characteristics of agricultural droughts using the VCI, TCI, and VHI drought indices from 2000 to 2018.
- Assess and analyze the correlations of SPI (3, 6, and 12 months) with VCI and VHI.

GRAPHICAL ABSTRACT

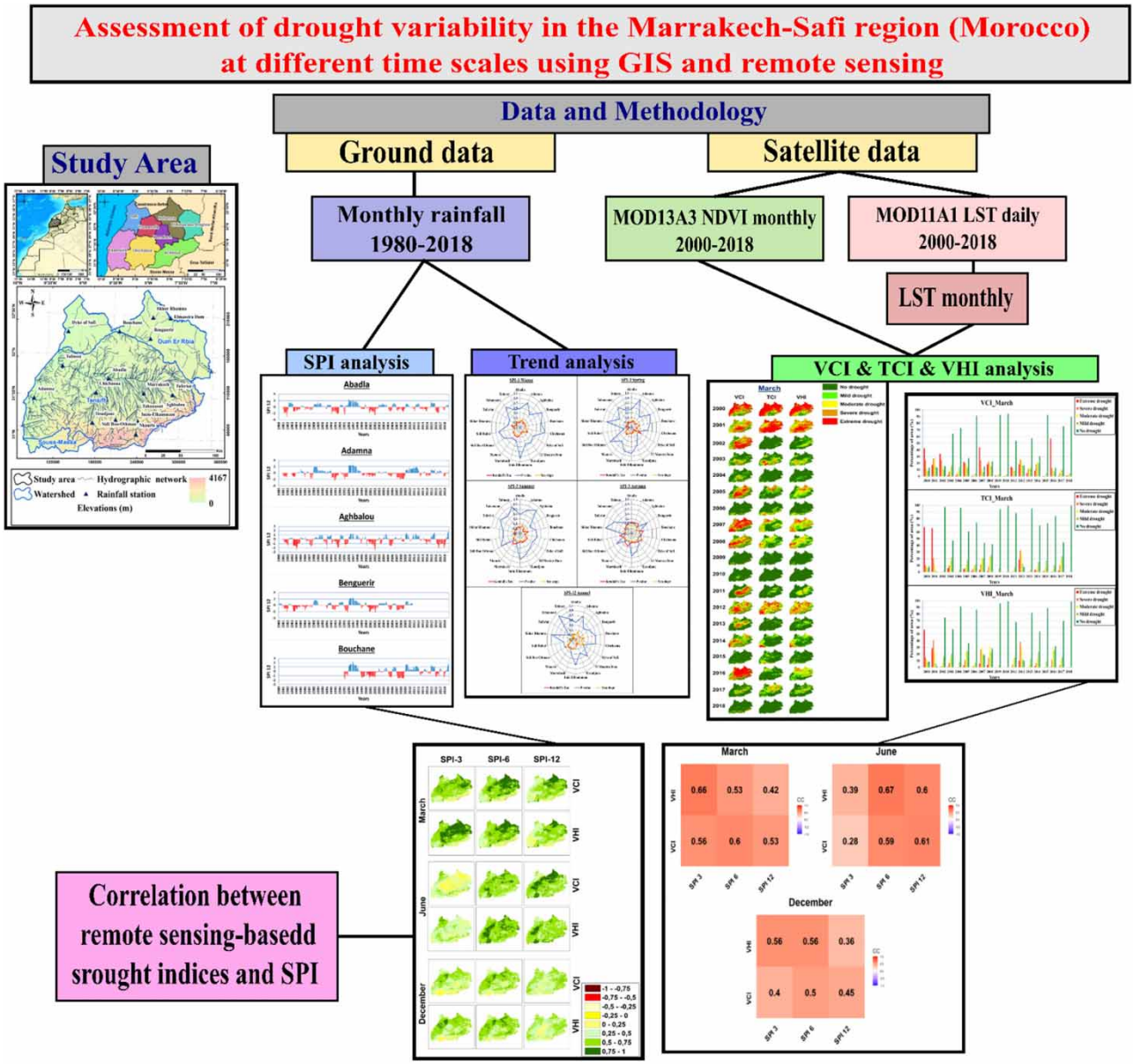

1. INTRODUCTION

Drought is a significant, complex, and recurrent environmental problem (Wilhite 2000). It occurs whenever regional hydrological variables, such as precipitation, snow cover, river flow, groundwater level, water storage, and soil moisture, are below normal (Dai 2010). All these variables are influenced, either directly or indirectly, by global warming, which our planet is currently experiencing, and its consequences strongly impact the social and economic conditions of populations by affecting various sectors of activity, such as agriculture, industry, energy, and the environment. Furthermore, it is essential to note that droughts directly impact surface and groundwater resources, resulting in a decrease in water supply and a general decline in water quality. They also lead to a deficit in soil moisture, reducing crop yields and grazing zones. Additionally, droughts decrease energy production (Mishra & Singh 2010; Fung *et al.* 2019).

Drought can be classified into four categories, as outlined by Mishra & Singh (2010): **(i) Meteorological drought** resulting from a prolonged shortage of precipitation or insufficient precipitation compared to normal levels (Elfatih & Eltahir 1992). Its

assessment is typically based on water levels recorded in rain gauges; **(ii) Agricultural drought** is often associated with a lack of soil moisture to meet crop and pasture needs (Heim & Richard 2002; Bravo *et al.* 2021); **(iii) Hydrological drought** results in a reduction in the level of groundwater, dams, rivers, and lakes compared to normal levels at different times (Mishra & Singh 2010; Delserone & Fleming 2013); **(iv) Socio-economic drought** is defined as the relationship between supply and demand for an economical product that requires precipitation (Mishra & Singh 2010). It occurs when demand exceeds supply due to insufficient water reserves related to meteorological conditions (Delserone & Fleming 2013).

Numerous studies have quantified drought characteristics, including intensity, duration, and frequency, using indices such as the standardized precipitation index (SPI) and the Palmer drought severity index (PDSI) (McKee *et al.* 1993; Li *et al.* 2016; Kim *et al.* 2021). These indices are essential for understanding and addressing drought-related problems. However, conventional methods for collecting and analyzing climatic data have limitations such as erroneous station observations, data collection delays, and irregular spatial distribution of ground stations with interrupted data records (Wang *et al.* 2015; Aksu *et al.* 2022b).

Remote sensing technology has revolutionized drought assessment by providing continuous spatial and temporal data for various drought indicators, including precipitation, temperature, vegetation cover, soil moisture, and evapotranspiration (AghaKouchak *et al.* 2015). This comprehensive information enhances our understanding of drought severity and its impacts on ecosystems and communities. Furthermore, remote sensing enables drought monitoring in remote and inaccessible areas where ground observations are limited or unavailable, making it a valuable resource for drought management decision-making, including crop planning and disaster response (AghaKouchak *et al.* 2015).

Beyond drought assessment, remote sensing data and high-resolution models, such as multispectral, thermal infrared, and microwave satellite imagery play crucial roles in various environmental domains, including wildfire assessment and management, flood risk evaluation, landslide monitoring, and storm risk analysis (AghaKouchak *et al.* 2015; Kulkarni *et al.* 2020; Chang *et al.* 2021). Additionally, they generate hazard maps that precisely identify at-risk areas based on an analysis of previous disasters, facilitating real-time monitoring and early warnings to mitigate impacts in various environmental contexts (Ezzine *et al.* 2014; Zeng *et al.* 2022; Aksu *et al.* 2022a).

Several indices are frequently employed to monitor drought in arid to semi-arid regions. Among them, we can mention the SPI (McKee *et al.* 1993), developed to quantify the precipitation deficit and monitor meteorological drought; the standardized precipitation and evaporation index (SPEI) (Vicente-Serrano *et al.* 2010) based on precipitation and evapotranspiration data, offering the possibility of identifying various types of drought and their impacts; the PDSI, developed by Palmer in 1965 to assess long-term drought (Dai 2011); the streamflow drought index (SDI) (Nalbantis & Tsakiris 2009), established to characterize the severity of hydrological drought; the standardized water-level index (SWI) (Bhuiyan 2004), used to quantify hydrological drought and assess groundwater recharge deficit. Regarding remote sensing-based indices, we mention those developed by Kogan (1995): the vegetation condition index (VCI), which has a high degree of accuracy in determining when the drought started, its severity, duration, and impact on vegetation; the temperature condition index (TCI) which allows measuring vegetation stress related to temperature and humidity, and finally, the vegetation health index (VHI) which is powerful in identifying, detecting, and monitoring agricultural drought.

The research conducted by Ayugi *et al.* (2022) highlights that North African countries, particularly Morocco, Algeria, and Tunisia, will be global hotspots with more intense and frequent droughts occurring during the 21st century. Due to its geographical position, Morocco is particularly vulnerable to climatic variations, experiencing droughts of varying severity levels at intervals of 3, 5, 15, and 30 years (World Bank 2013; Hadria *et al.* 2019). These climatic events can worsen in the future, causing significant material and human damage (World Bank 2013) and an important imbalance between water supply and demand (Hadri *et al.* 2022; Saouabe *et al.* 2022). Several studies have been conducted in Morocco to monitor and analyze drought trends in this alarming context. However, in the Marrakech-Safi (MS) region, which is particularly affected, there are still many gaps in the studies related to drought monitoring. The research (Ezzine *et al.* 2014; Hadria *et al.* 2019) focuses on the region's meteorological and agricultural drought indices. Hadri *et al.* (2021a) examine the spatial and temporal relationships between vegetation activity and drought severity at different times of the year using Landsat satellite images and indices such as SPI and SWI. The research of Zkhiri *et al.* (2018) focuses on characterizing current and future drought in the High Atlas basins using the SPI index and a set of regional climate model simulations.

Our study aims to improve our understanding of drought risk and our capacity to assess it by integrating data from various sources, such as satellites, rainfall, and thematic data. We will seek to answer several questions regarding meteorological and agricultural drought characterization using statistical methods and remote sensing. Additionally, we aim to provide a

scientific basis for planning and predicting drought events to support decision-makers and stakeholders in developing risk mitigation and adaptation strategies. The specific objectives of our study are as follows: 1 – Deepen our understanding of the spatial and temporal variability of meteorological droughts by using the SPI for 3, 6, and 12 months from 1980 to 2018. 2 – Analyze seasonal and annual trends in the SPI by employing the Mann–Kendall (MK) test and Sen's slope estimator. 3 – Monitor agricultural drought in the region using the VCI, temperature condition index (TCI), and VHI drought indices with a spatial resolution of 1 km during the period from 2000 to 2018. 4 – Establish correlations between the SPI (3, 6, and 12 months) and the VCI and VHI indices for March, June, and December to better understand the relationships between meteorological and agricultural drought.

2. MATERIALS AND METHODS

2.1. Study area

The MS region, located in west-central Morocco on the Atlantic coast, covers an area of 39,167 km^2 (5.5% of the country's surface area). Its population is estimated at 4.521 million habitants, representing 13.36% of the country's total population (CERED & HCP 2017).

Currently, the region consists of the prefecture of Marrakech as its capital, along with seven provinces: Al Haouz, Chichaoua, El Kelâa des Sraghna, Essaouira, Rehamna, Safi, and Youssoufia. It encompasses 251 communes, including 23 urban and 228 rural areas (CERED & HCP 2017). Geographically, it is surrounded by the Greater Casablanca-Settat region to the north, the region of Beni Mellal-Khenifra in the east, the region of Drâa-Tafilalet in the southeast, the region of Souss-Massa in the south, and the Atlantic Ocean is in the west (Figure 1). The topography of the MS region exhibits various natural morphological units (Figure 1). The region includes the plateau area, which comprises the Rehamna and Bahira plateaus, featuring a moderate altitude relief. The plains area encompasses the plains of Abda and Rehamna, characterized by a relatively flat or slightly undulating topography, with maximum elevations not exceeding 500 m. Additionally, the Haouz plain is part of this region, bounded to the north by the Tensift River and the Jebilet mountains, to the west by the Chichaoua River, and to the east by the high Atlas Mountains. The Jebilet chain is a mountainous region spanning 170 km, with altitudes ranging from 300 to 1,000 m. It extends from the Mouissate region in the west to the central High Atlas in the east (JICA *et al.* 2008).

Furthermore, the mountain zone comprises the High Atlas Mountains, located south of the Haouz plain. These mountains encompass peaks exceeding 3,000 m, with Jbel Toubkal as the highest at 4,167 m. The valleys of these mountains are the origin of the tributaries of the Tensift River (JICA *et al.* 2008). Lastly, the Chichaoua-Essaouira basin represents a rugged plateau west of the Haouz plain.

The region has a highly varied climate, characterized by three climates: arid and semi-arid across most of the region and sub-humid in the High Atlas. It is influenced by the high Atlas Mountains range and the Atlantic Ocean (through the cold current from the Canary Islands), with an average maximum temperature of around 37.7 °C and a minimum of about 4.9 °C. There is also significant variability in rainfall across the region, although it remains low and irregular, ranging from 800 mm in the high Atlas to 190 mm in the plains (DGCL 2015).

The MS region is characterized by the presence of two watersheds: the large Tensift watershed and a portion of the Oum Er-Rbia watershed, formed by several sub-watersheds (Rdat, Zat, Ourika, Nfis, Assif El Mal, Chichaoua, Ksob, Igouzoulen, Tassaout, and Lakhdar). These sub-watersheds receive rainfall and snowfall, contributing to the overall water resources of the region (DGCL 2015). It also has eight large and medium dams. These are Al Massira, Sidi Driss, Lalla Takerkoust, Yacoub El Mansour, Abou El Abbas Sebti, Jazouli, My Youssef, and Dyke of Safi. These dams provide urban and rural populations with drinking water, electricity, and irrigation.

In recent decades, the region has witnessed a significant decline in rainfall, leading to increased drought occurrences. Research conducted by Fniguire *et al.* (2017) indicated that these drought events, characterized by insufficient precipitation over 12- to 24-month periods starting in 1975, have become more frequent and prolonged. Lkammarte *et al.* (2023) documented moderate drought from 1980 to 1986, followed by alternating dry and wet years. In contrast, 1996–1997 saw unusually wet conditions, but a persistent drought from 1998 to 2001 quickly followed. Najmi *et al.* (2023) identified 13 drought episodes during the 2007–2019 study period, with the longest lasting 12 months. Additionally, Bouras *et al.* (2020) emphasized the significant impact of agricultural drought on wheat yields in the region.

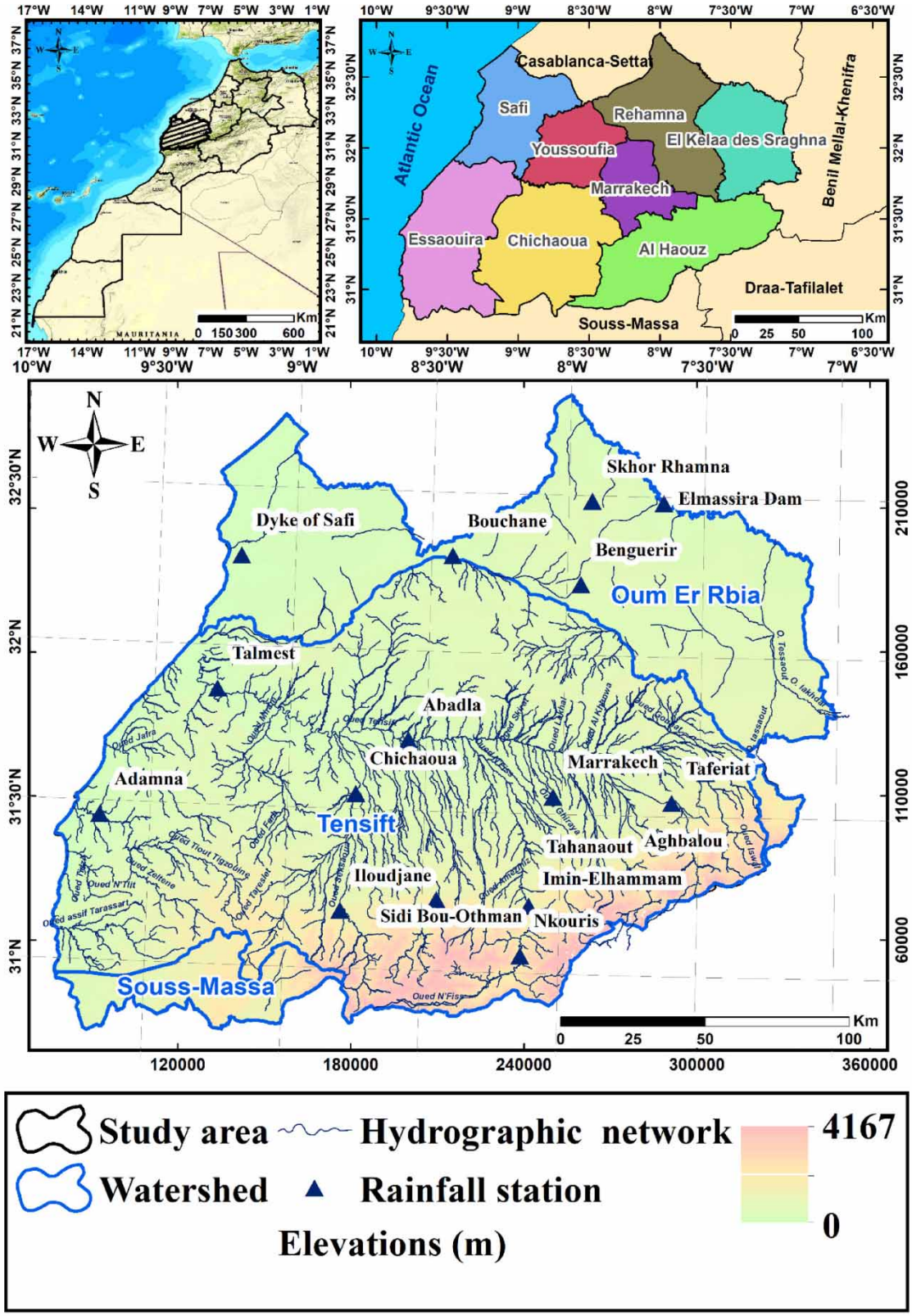

Figure 1 | Location of the study area in the Marrakech-Safi region in Morocco.

2.2. Data

2.2.1. Rainfall data

The present study relies on monthly rainfall data from 18 stations, covering the period from 1980 to 2018. These data were obtained from the Tensift Hydraulic Basin Agency (ABHT) and the Oum Er-Rbia Hydraulic Basin Agency (ABHOER). It is important to note that the rainfall data for each station are not homogeneous in terms of the study period. Several factors contribute to temporal variability, including commissioning certain stations at different times, stations no longer in service, maintenance work, and missing data due to technical problems or breakdowns affecting data collection (Table 1).

We conducted rigorous data quality control with the assistance of hydraulic basin agencies to address missing data, outliers, duplicates, abrupt changes, and other anomalies to ensure data integrity, quality, and reliability. Additionally, we performed a homogeneity test, employing the standard normal homogeneity test, Pettitt test, and quantile matching (QM) on the rainfall data. This step aimed to verify consistent data collection practices, ensuring no significant alterations in measurement conditions or station locations. Similar statistical tests were employed by Hadri *et al.* (2021b) in Chichaoua-Mejjate, Morocco, and by Aksu *et al.* (2022b) in the Black Sea region, Turkey. The outcomes of these tests collectively affirm the homogeneity of the data, providing a solid foundation for their reliable use in subsequent statistical analysis and forecasts.

2.2.2. Remote sensing data

Concerning the satellite data, we selected monthly data from the TERRA/AQUA satellite, which incorporates the MODIS sensor. The MODIS sensor is widely recognized in the scientific community for its applications in Earth system studies, providing multi-year data across a broad spectral range, spanning from visible (VIS) to long-wave infrared (LWIR) (Barnes & Salomonson 1992; Barnes *et al.* 2003). It uses a comprehensive suite of onboard calibrators (OBCs), which have not been employed in any remote sensing instrument before (Sun *et al.* 2003; Xiong *et al.* 2005; Xiong & Barnes 2006). It has generated over 40 scientific datasets (Esaias *et al.* 1998; Justice *et al.* 1998; Salomonson *et al.* 2002; King *et al.* 2003), some of which have undergone geometric and radiometric corrections.

For our study area, we selected the period from 2000 to 2018 to calculate the drought indices based on several factors. First, we considered the availability and suitability of the data, ensuring that we had a comprehensive dataset for analysis.

Table 1 | Characteristics of the rainfall stations in the MS region

N°	Stations	Coordinates		Altitudes (m)	Measuring periods	Duration (years)
		X (m)	*Y* (m)			
1	Abadla	−8.56594042	31.7218077	245	1980–2018	39
2	Adamna	−9.68252883	31.456299	71	1980–2018	39
3	Aghbalou	−7.74572429	31.3144996	1042	1980–2018	39
4	Benguerir	−7.9492	32.22161	471	1980–2015	36
5	Bouchane	−8.42235	32.30139	277	1994–2018	25
6	Chichaoua	−8.75236	31.54862	344	1980–2018	39
7	Dyke of Safi	−9.19937	32.28241	85	1980–2018	39
8	Elmassira Dam	−7.65022	32.48088	247	1985–2017	33
9	Iloudjane	−8.79647	31.18123	752	1989–2018	30
10	Imin-Elhammam	−8.11088	31.21189	742	1980–2018	39
11	Marrakech	−8.03154	31.55526	460	1980–2018	39
12	Nkouris	−8.13793286	31.0551429	1059	1980–2018	39
13	Sidi Bou-Othman	−8.44735764	31.2239129	816	1989–2018	30
14	Sidi Rahal	−7.47563594	31.6388841	688	1980–2018	39
15	Skhor Rhamna	−7.91367212	32.4832361	476	1980–2015	36
16	Taferiat	−7.59926108	31.5431877	759	1983–2018	36
17	Tahanaout	−7.96296111	31.2919464	1043	1980–2018	39
18	Talmest	−9.27002151	31.8632272	34	1985–2018	34

Additionally, the high resolution of the satellite images provided by MODIS was a crucial factor in our decision. Lastly, the MODIS sensor has been operational since February 2000 and continues to provide data up to the present day. Specifically, we obtained the EVI (enhanced vegetation index) and LST (land surface temperature) MODIS data from the MOD13A3 and MOD11A1 products. These data were downloaded from the official source, The United States Geological Survey (USGS) website at https://earthexplorer.usgs.gov/ (USGS 2021). The MOD13A3 data, a monthly level 3 gridded product, has a spatial resolution derived from surface reflectance corrected for molecular scattering, ozone absorption, and aerosols (Table 2) (Didan *et al.* 2015). On the other hand, the MOD11A1 data provide daily LST and emissivity per pixel in a 1,200 by 1,200 km grid with a 1 km resolution. It includes additional information, such as quality control assessments, observation hours, day and night surface temperature bands, view Zenith angles, precise sky coverages, and emissivity bands for 31 and 32 land cover types (Table 2) (Wan 2013).

2.3. Methodology

2.3.1. Standardized precipitation index

SPI is an index described and developed by McKee *et al.* (1993) to detect, determine, and characterize the intensity and frequency of drought at different time scales (1, 3, 6, 9, 12, and 24 months). The widespread use of this index can be attributed to its straightforward computation compared to alternative indices, its dependence on just one variable (precipitation), and its proficiency in identifying the start and end of drought (Angelidis *et al.* 2012). The SPI quantifies the precipitation deficit and its impacts on groundwater, reservoir storage, snowpack, streamflow, and soil moisture (Tsakiris & Vangelis 2004). It is derived using a gamma probability distribution based on observed precipitation data over a long-time scale.

To ensure precise computation of the SPI index, possessing a minimum of 30 years of monthly data is crucial, recognized as the optimal temporal duration (Guttman 1994). Thus, by focusing on the preceding three decades, we guarantee the availability of a dataset that is both extensive and resilient enough to conduct SPI computations with efficacy.

The calculation of SPI is typically performed by comparing the precipitation on a specific time scale to the mean value of the series and then dividing this difference by the standard deviation of the series. The mathematical expression is as follows (Alsenjar *et al.* 2022):

$$\mathbf{SPI}_{ij-k} = \left(\frac{x_{ij} - \mu_j}{\sigma_j}\right) \tag{1}$$

X_{ij} represents recorded precipitation, where i represents the year (1 to n) and j represents the month (1–12). μ_j and σ_j denote the mean and standard deviation of precipitation in month j, respectively.

Because population parameters are unknown in Equation (1), we use the probability approach to calculate the SPI value. To achieve this, we determine the probability density function for the precipitation data series. Our approach is as follows:

$$g(x) = \frac{1}{\beta^{\alpha}\,\Gamma(\alpha)}\; x^{\alpha-1} e \frac{-x}{\beta}, \quad x > 0 \tag{2}$$

Table 2 | Characteristics of MODIS

	MOD13A3	MOD11A1
Characteristic	NDVI MODIS	LST MODIS
Spatial resolution	1 km	1 km
Temporal resolution	Monthly	Daily
Coordinate system	Sinusoidal	Sinusoidal
Period	February 2000 – Present	February 2000 – Present

The parameters α and β represent the shape and scale, respectively. The gamma function is defined as (Alsenjar *et al.* 2022):

$$\Gamma(\alpha) = \int_0^{\infty} x^{\alpha-1} e^{-x} dx \tag{3}$$

The estimated optimal values for α and β are as follows:

$$\alpha = \frac{1}{4A}\left(1 + \sqrt{1 + \frac{4A}{3}}\right)$$

$$\beta = \frac{\bar{x}}{\alpha} \tag{4}$$

$$A = \ln(\bar{x}) - \frac{\sum \ln(x)}{n}$$

where n represents the number of years in the precipitation series, the following equation calculates the cumulative probability for month j:

$$G(x) = \int_0^{x} g(x) dx = \frac{1}{\beta^{\alpha}\Gamma(\alpha)} \int_0^{\kappa} x^{\alpha-1} e^{\frac{-x}{\beta}} dx \tag{5a}$$

$$H(x) = q + (1 - q)G(x) \tag{5b}$$

$$\mathbf{SPI} = S\left(t - \frac{c_0 + c_1 t + c_2 t^2}{1 + d_1 t + d_2 t^2 + d_3 t^3}\right) \tag{6}$$

$$t = \begin{cases} \sqrt{\ln\left(\frac{1}{H(x)}\right)^2}, & \text{for } 0 < H(x) \leq 0.5 \\ \sqrt{\ln\left(\frac{1}{1.0 - H(x)}\right)^2}, & \text{for } 0.5 < H(x) < 1.0 \end{cases} \tag{7}$$

The constants are $C_0 = 2.515517$, $C_1 = 0.802853$, $C_2 = 0.020328$, $d_1 = 1.432788$, $d_2 = 0.189269$, and $d_3 = 0.001308$, where q is the probability of zeroes, $H(x)$ in Equation (5b) represents the cumulative probability, and $S = 1$ if $H(x) > 0.5$, otherwise $S = -1$. Equations (6) and (7) are then used to turn the cumulative probability $H(x)$ into the standard normal random variable Z, with a mean of zero and a variance of one. This value represents the SPI (Alsenjar *et al.* 2022). The classification of drought based on the SPI values is presented in Table 3.

Table 3 | Drought classification based on SPI value (Caccamo *et al.* 2011)

SPI value	Classification
SPI ≥ 2,00	Extremely wet
1,50 ≤ **SPI** < 2	Severely wet
1,00 ≤ **SPI** < 1,50	Moderately wet
− 1< **SPI** < 1	Near normal
− 1,50 < **SPI** ≤ − 1,00	Moderate drought
− 2 < **SPI** ≤ − 1,50	Severe drought
SPI ≤ − 2	Extreme drought

2.3.2. Vegetation condition index

VCI is an index used to assess vegetation moisture conditions (Kogan 2000) and monitor agricultural drought. This parameter demonstrates a strong ability to detect drought and measure its duration, severity, occurrence, and impact on vegetation. As a result, it provides reliable information regarding both short-term and long-term drought events, regardless of whether they are well-defined or indefinite (Kogan 1995). The calculation equation for VCI is as follows:

$$\mathbf{VCI} = \frac{\mathbf{NDVI} - \mathbf{NDVI_{min}}}{\mathbf{NDVI_{max}} - \mathbf{NDVI_{min}}} * 100 \tag{8}$$

with:

NDVI: The NDVI for the study period;
$\mathbf{NDVI_{min}}$: The minimum NDVI for the study period, calculated from historical data;
$\mathbf{NDVI_{max}}$: The maximum NDVI for the study period also calculated from historical data.

2.3.3. Temperature condition index

TCI is an index that utilizes LST, estimated from the AVHRR thermal infrared band (channel 4). It is instrumental in determining temperature-related drought and excessive moisture stress (Kogan 1995). The TCI is defined as follows:

$$\mathbf{TCI} = \frac{(\mathbf{LST_{max}} - \mathbf{LST})}{(\mathbf{LST_{max}} - \mathbf{LST_{min}})} * 100 \tag{9}$$

with:

LST: The land surface temperature of the studied period in Kelvin;
$\mathbf{LST_{min}}$: The minimum land surface temperature of the study period, calculated from historical data (K);
$\mathbf{LST_{max}}$: The maximum land surface temperature of the study period, calculated from historical data (K).

2.3.4. Vegetation health index

VHI is an index developed by Kogan (1995). It combines two other indices, VCI and TCI, based on the negative correlation between vegetation stress and temperature (Justice *et al.* 1998). This index effectively identifies, understands, classifies, provides early warning, monitors, and assesses the frequency and intensity of agricultural drought (Seiler *et al.* 1998). The VHI is defined as follows (Table 4):

$$\mathbf{VHI} = \mathbf{0.5VCI} + \mathbf{0.5TCI} \tag{10}$$

2.3.5. Statistical test for trend analysis

The MK test is a widely used nonparametric approach for analyzing hydrological and climate data, recommended by the World Meteorological Organization (WMO) for its ability to handle missing values and robustness against outliers (Jamro *et al.* 2020).

Table 4 | Drought classification based on VCI, TCI, and VHI values (Kogan 1995)

	TCI value	VHI value	Classification
$40 < \mathbf{VCI} \leq 100$	$40 < \mathbf{TCI} \leq 100$	$40 < \mathbf{VHI} \leq 100$	No drought
$30 < \mathbf{VCI} \leq 40$	$30 < \mathbf{TCI} \leq 40$	$30 < \mathbf{VHI} \leq 40$	Mild drought
$20 < \mathbf{VCI} \leq 30$	$20 < \mathbf{TCI} \leq 30$	$20 < \mathbf{VHI} \leq 30$	Moderate drought
$10 < \mathbf{VCI} \leq 20$	$10 < \mathbf{TCI} \leq 20$	$10 < \mathbf{VHI} \leq 20$	Severe drought
$\mathbf{VCI} \leq 10$	$\mathbf{TCI} \leq 10$	$\mathbf{VHI} \leq 10$	Extreme drought

This test is employed to identify significant trends in hydrometeorological time series, whether they are increasing or decreasing. Initially proposed by Mann (1945) and later statistically formulated by Kendall (1975), the MK test has been utilized to detect trends in various climatic parameters, including precipitation, evaporation, evapotranspiration, temperature, streamflow, and the SPI (Malik *et al.* 2020; Pathak & Dodamani 2020).

In this study, the MK trend test and the Sen slope estimator were used to analyze the nonlinear trends of the SPI index at each station on both an annual and seasonal time scale. The seasons were categorized as follows: winter (December, January, and February), spring (March, April, and May), summer (June, July, and August), and autumn (September, October, and November). The test results (Kendall's tau, *P*-value, and Sen's slope) were calculated using XLSTAT 2021, with a significance level of 5% and a confidence interval of 95%. At this significance level, a negative trend is considered statistically significant if its *P*-value is ≤ 0.05, and a positive trend is considered statistically significant if its *P*-value is ≥ 0.05 (Yue & Pilon 2004).

The calculation of the MK test follows the formula:

$$\boldsymbol{S} = \sum_{\boldsymbol{i}=1}^{\boldsymbol{N}-1} \sum_{\boldsymbol{J}=\boldsymbol{i}+1}^{\boldsymbol{N}} \boldsymbol{sgn}\,(\boldsymbol{xj} - \boldsymbol{xi}) \tag{11}$$

where N represents the number of measurements in a time series, xj, and xi denote the values in the time series. The sign function « *sgn* » is represented by:

$$\boldsymbol{sgn}\,(\boldsymbol{xj} - \boldsymbol{xi}) = \begin{cases} +1, & f\,(xj - xi) > 0 \\ 0, & if\,(xj - xi) = 0 \\ -1, & if\,(xj - xi) < 0 \end{cases} \tag{12}$$

The statistic S represents the difference between positive and negative differences. When the number of samples 'N' exceeds 8, S approaches a normal distribution with a mean of $E(\boldsymbol{S}) = \boldsymbol{0}$.

The following formula determines the variance of the MK test and the significance test Z:

$$\mathbf{Var}\,(\boldsymbol{S}) = \frac{\boldsymbol{n}\,(\boldsymbol{n}-1)(2\boldsymbol{n}+5) - \sum_{\boldsymbol{i}=1}^{\boldsymbol{m}} \boldsymbol{ti}\,(\boldsymbol{i})(\boldsymbol{i}-1)(2\boldsymbol{i}+5)}{18} \tag{13}$$

$$\boldsymbol{Zc} = \begin{cases} \dfrac{\boldsymbol{S}-1}{\sqrt{\mathbf{Var}\,(\boldsymbol{S})}}, & \text{for } S > 0 \\ 0, & \text{for } S = 0 \\ \dfrac{\boldsymbol{S}+1}{\sqrt{\mathbf{Var}\,(\boldsymbol{S})}}, & \text{for } S < 0 \end{cases} \tag{14}$$

In the above equation, n represents the number of linked groups, and ti represents the number of data points in the ith linked group.

The value of Zc is utilized to assess the significance of the trend. If $Zc > 0$, it indicates an increasing trend, while $Zc < 0$ suggests a decreasing trend. A significance level α is employed to determine whether the trend is monotonic increasing or decreasing. If $Zc > Z\,\alpha/2$, the trend is considered statistically significant, and vice versa (Junaid 2021).

The slope of the trend is estimated using Sen's slope estimator, a robust nonparametric method (Gao *et al.* 2020).

$$\boldsymbol{\beta} = \text{median}\left(\frac{\boldsymbol{xj} - \boldsymbol{xi}}{\boldsymbol{j} - \boldsymbol{i}}\right), \quad \text{j} > \text{I} \tag{15}$$

where β represents the estimate of Sen's slope, a positive value indicates an upward trend in the series, while a negative value suggests a downward trend during the considered period.

2.3.6. Spatial interpolation

In this study, we employed the inverse distance weighted (IDW) interpolation method to map the SPI1, SPI3, SPI6, and SPI12 parameters in the MS region using ArcGIS 10.2 software. This technique supposes estimating the value at an unknown

location as a weighted average based on the distance between known and available points (Ikechukwu *et al.* 2017; Liu *et al.* 2020). The IDW method is highly recommended over the Kriging method due to its computational efficiency and suitability for spatially interpolating meteorological parameters (Gumus *et al.* 2021; Habibi & Meddi 2021). We performed the interpolation using the following equation (Habibi & Meddi 2021):

$$Z(X) = \frac{\sum_{j=1}^{m} Z\,(xi) d_{ij}^{-w}}{\sum_{j=1}^{m} d_{ij}^{-w}} \tag{16}$$

where w represents the weighting parameter, d_{ij} is the distance between the observed and predicted values' locations.

2.3.7. Correlation analysis

We conducted Pearson correlation analysis to evaluate the performance of remote sensing-based indices for drought monitoring. This statistical method examines the linear relationship between two continuous variables, specifically focusing on the associations between VCI, VHI, and SPI at different time scales. The correlation analysis was independently performed for March, June, and December, comparing the three remote sensing-based drought indices with the corresponding SPI values (3, 6, and 12 months) calculated for the same months (Figure 2).

The correlation coefficient r determines Pearson correlation classification. When r is close to 1, this indicates a strong positive correlation; when r is close to 0, this shows no correlation; when r is close to −1, this means a strong negative correlation.

3. RESULTS AND DISCUSSION

3.1. SPI analysis and drought characteristics

This study examined the annual SPI of each rainfall station in the MS region from 1980 to 2018. A negative SPI-12 value indicates drought conditions, whereas a positive SPI-12 value indicates wet conditions. We have presented selected examples of results from specific stations representing the various geomorphological and agricultural schemes in the study area rather than including data from all stations within our study region.

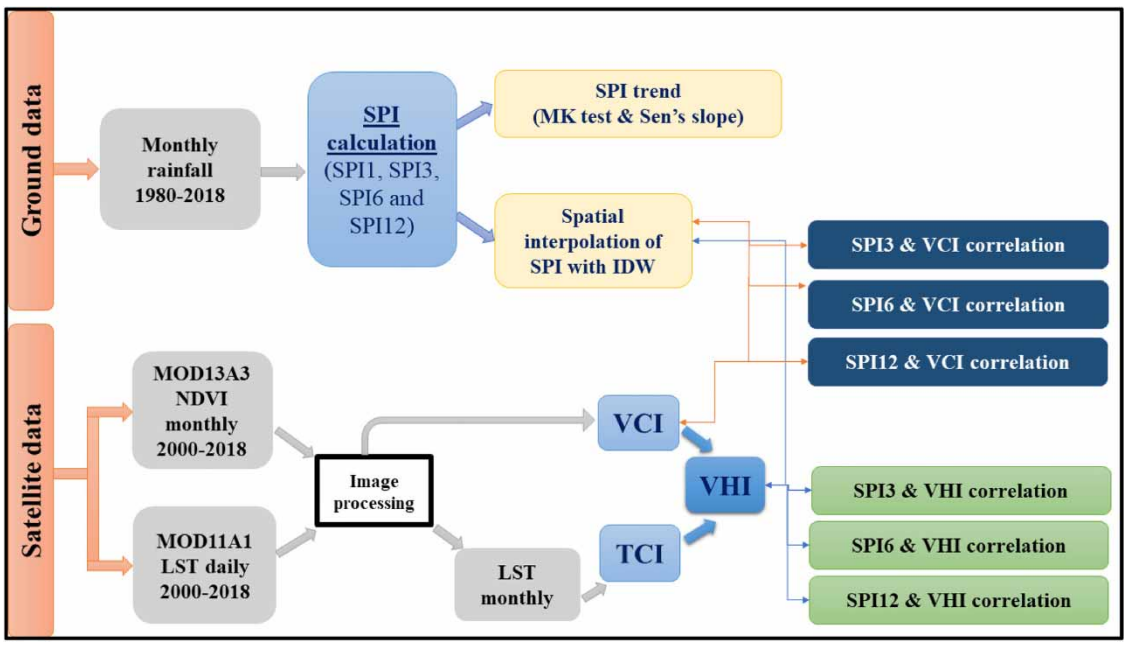

Figure 2 | Methodological schema of the study.

Analysis of the SPI-12 results revealed that these stations experienced alternating periods of drought, wetness, and normal conditions throughout the study period (Figures 3 and 4).

At the **Abadla station** on the **Haouz plain**, the SPI-12 results from 1980 to 2018 revealed alternating periods of dryness, wetness, and normal conditions. Severe to extreme drought conditions were observed during 1980–1982, 1991–1993, 1995, 2000–2002, 2005, 2008, 2012–2014, and 2015–2017, with SPI-12 values reaching −1.57, −2.17, and −3, respectively, indicating significant rainfall deficits. In contrast, 1988–1989, 1996–1999, and 2013–2014 were wet periods indicated by positive SPI-12 values, signifying rainfall surpluses. The remaining years generally exhibited near-normal rainfall (Figure 3). Moving to the **Adamna station** in the **Chichaoua-Essaouira basin**, the annual SPI index from 1980 to 2018 showed significant long-term dry periods observed from 1980 to 1984 and 1998 to 2002, represented by moderate droughts. The years 1991–1995 and 2004–2009 had large SPI values, indicating severe and extreme droughts ranging from −1.5 to −2.56. In addition, the SPI2 index showed four prolonged wet sequences between 1988 and 1991, 1996 and 1999, 2009 and 2011, and 2014 and 2016 (Figure 3). At the **Aghbalou station**, located in the **foothills of the High Atlas**, during the period from 1980 to 2018, we observed an alternation between moderately to severely dry years and wet to normal years. This result indicates variability in climatic conditions, with some years displaying varying drought levels. In contrast, the other years were characterized by normal humidity or precipitation levels (Figure 3). At **Benguerir station**, which is located in the **plateau zone**, the annual SPI index reveals a predominance of dry years, particularly during the periods 1983–1987, 1998–2003, and 2006–2008. These years exhibited severe and extreme drought conditions, with SPI values reaching low values (−2.26). In contrast, the periods 1980–1982 and 1996–1999 were characterized by relatively wet to extremely wet conditions (Figure 3). Similarly, the **Bouchane station** in the same area also demonstrated an alternation between dry and wet periods. Prolonged droughts lasting 2 and 3 years were observed in 1994, 1998, and 2007, respectively. On the other hand, the periods from 1996 to 1998 and 2008 to 2012 were marked by extremely wet conditions (Figure 3). The **Dyke of Safi station** is located in a **coastal zone**. The 1980s were primarily characterized by a prolonged, severe to extreme 5-year drought, followed by alternating years of surplus and deficit rainfall (Figure 4). **Marrakech station** experienced a sequence of wet and dry years. In 1981, moderate to severe drought conditions were predominant. However, there was a notable exception of an extended and exceptionally wet period between 1995 and 1999 (Figure 4). At the **Skhor Rhamna station**, located on the **Rehamna plain**, the SPI-12 results for each year from 1980 to 2010 reveal alternating periods of dryness, wetness, and normal conditions. The years 1981, 1983–1984, 1994, 1998, 2001, 2005, and 2007 were identified as moderate to severe drought periods. In contrast, 1987–1988, 1991, 1995–1997, and 2008–2010 were marked by generally wet to very wet weather conditions. Other years were considered normal (Figure 4). At **Taferiat station**, in a **mountainous area**, dry years predominated from 1988 to 2018, with precipitation deficits observed from 2000 to 2003, 2004 to 2009, 2013 to 2015, and 2016 to 2018. The SPI-12 values reached −2.7, indicating severe drought during these periods. However, an exceptionally wet period was observed from 1994 to 1998, with a significant excess of precipitation (Figure 4). At the **Talmest station**, located in the **Chichaoua-Essaouira basin**, the SPI-12 results for the period 1986–2009 indicate varying conditions. Specific years, such as 1988–1990 and 1996–1998, were characterized by wet conditions. In contrast, other years, including 1985–1987, 1991–1993, 1994–1995, 1999–2002, and 2006–2008, experienced dry conditions (Figure 4).

Figure 5 and Table 5 display data on the frequency of drought occurrences, categorized according to the SPI, recorded at various rainfall monitoring stations. Our findings revealed that moderate drought was most prevalent in the plateau zone (El Massira Dam 13.19%), the Haouz plain (Chichaoua 12.14%), and the plateau zone (Bouchane 11.04%). Conversely, severe drought was more frequently observed in the mountainous area (Nkouris 8.32%), the Rhamna plain (Skhor Rhamna 7.10%), and the foothills of the high Atlas (Sidi Bou-Othman 7.04%). Additionally, extreme drought events are more commonly reported in the Chichaoua-Essaouira basin (Adamna and Talmest), with respective percentages of 4.81 and 4.11, as well as in mountainous regions (Taferiat 3.13%). The results underscore the substantial influence of topography and precipitation patterns on drought occurrence in each region. Nonetheless, when conducting drought risk assessments, it remains critical to account for topography and other meteorological factors.

The findings align with Hadri *et al.* (2021a) and Ouassanouan *et al.* (2022), who observed alternating dry and wet years in similar contexts, such as Chichaoua-Mejjeate and the high Atlas, both within the MS region. Our study emphasizes the role of topography in drought vulnerability, with various geomorphological zones in the MS region showing distinct patterns. These findings fit with what other researchers have found in the Tensift basin, which covers a large part of the MS region (Fniguire *et al.* 2017; Habitou *et al.* 2020; Najmi *et al.* 2023) that topography affects the vulnerability of populations to drought due to changes in the location and timing of rainfall. The north-south gradient further influences drought vulnerability in Morocco

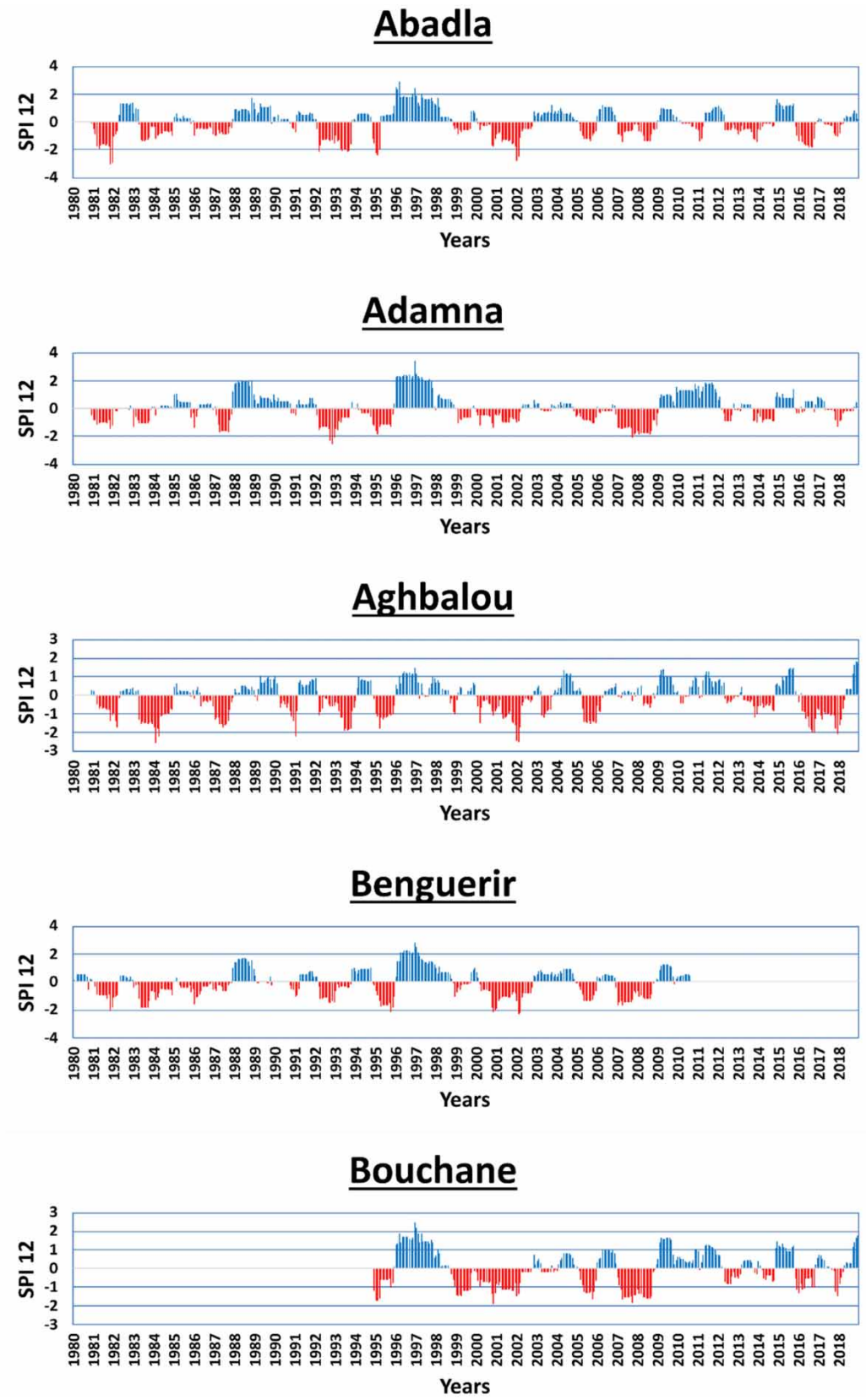

Figure 3 | Evolution of the drought using annual SPI in the different stations of Marrakech-Safi (for example).

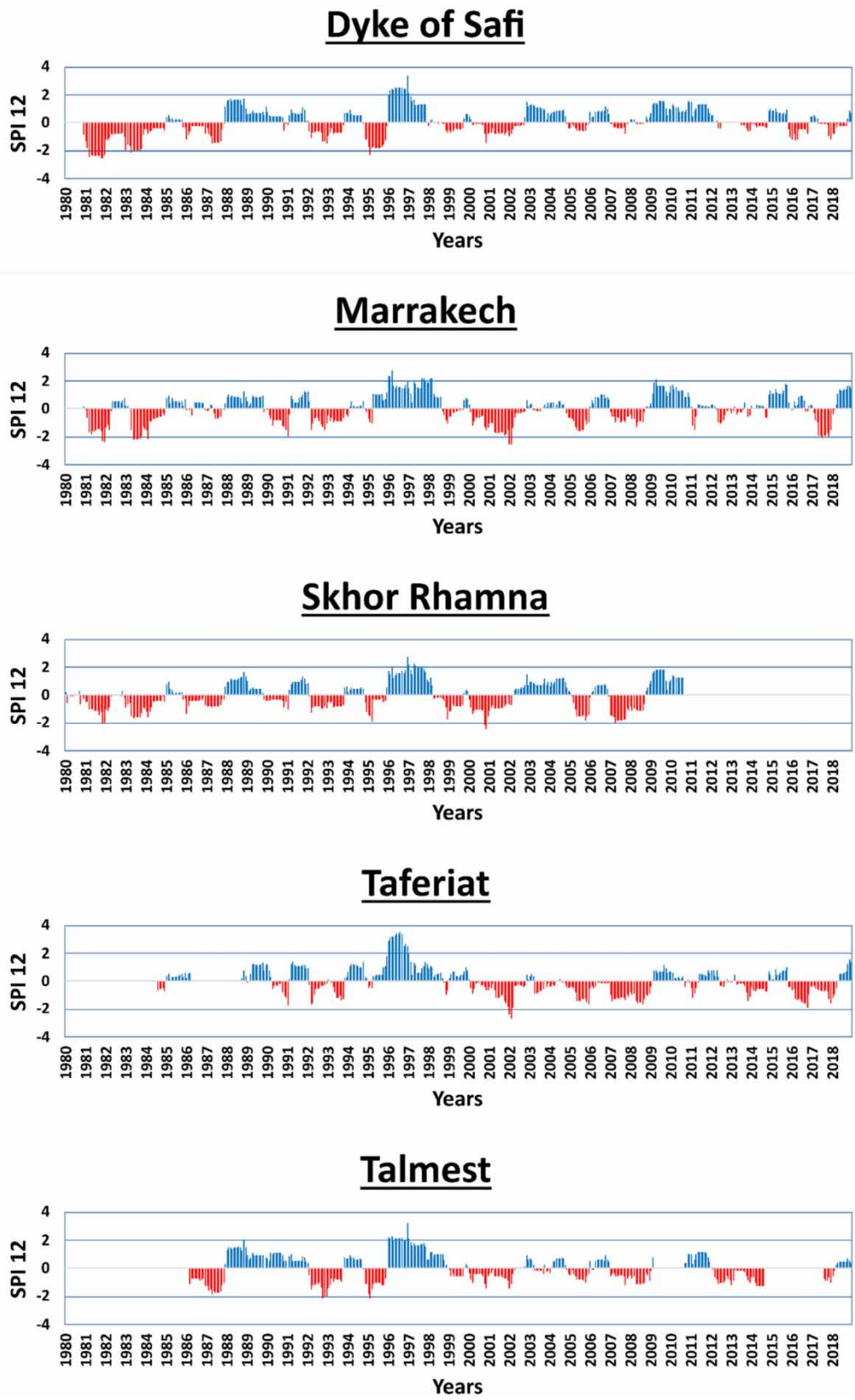

Figure 4 | Evolution of the drought using annual SPI in the different stations of Marrakech-Safi (for example).

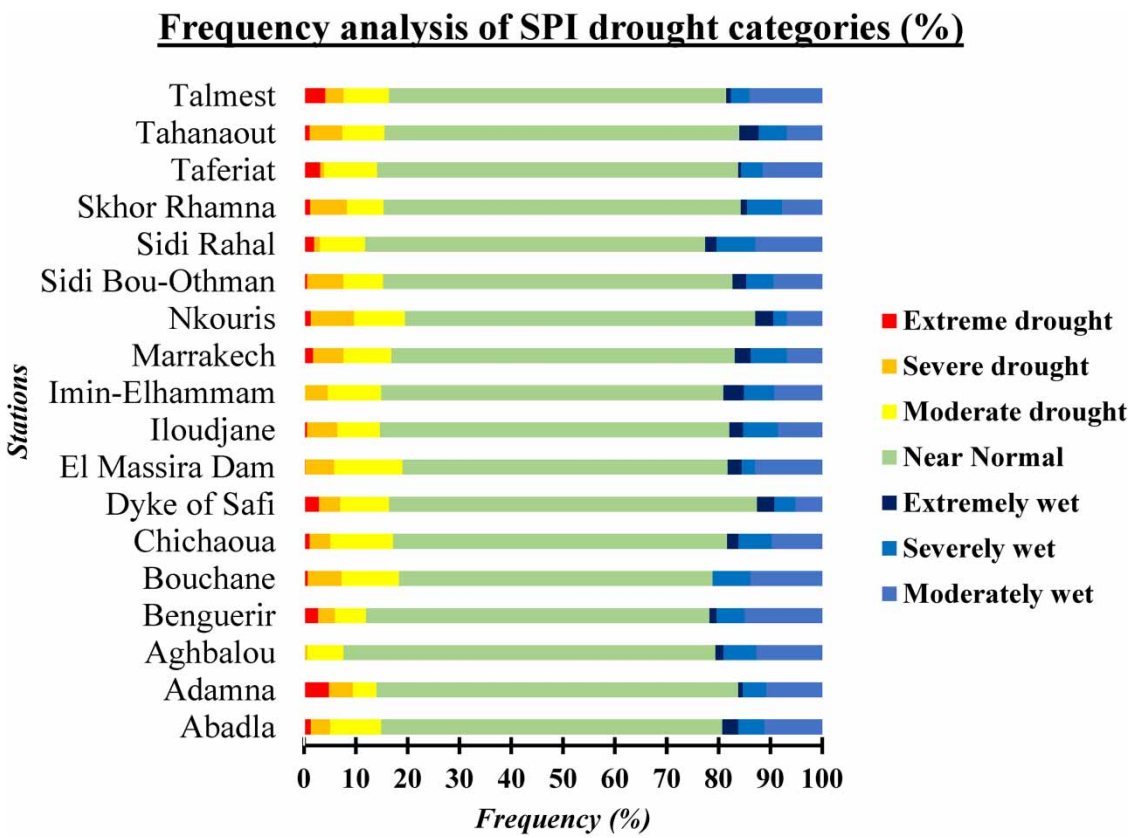

Figure 5 | Frequency analysis of SPI drought categories (%) – stacked bar chart.

(Fniguire *et al.* 2017; Almazroui *et al.* 2020; Ouatiki *et al.* 2023), where the northern region (low altitudes) experiences lower vulnerability due to higher rainfall proximity to the Atlantic Ocean. In contrast, the western and eastern regions (higher altitudes) face heightened vulnerability due to reduced rainfall and higher temperatures.

Moreover, the continental climate significantly increases drought vulnerability in the MS region, particularly in the Haouz plain, where reduced precipitation, elevated temperatures, and evaporation contribute to the risk (Fniguire *et al.* 2014; Bennani *et al.* 2016). Climate change and variability have led to rainfall deficits, posing a substantial drought risk in central Morocco. According to historical data, there were five wet cycles between 1926 and 1975, three lengthy dry cycles after 1975, and SPI values show an increase in the frequency and severity of meteorological drought over the previous four decades (Fniguire *et al.* 2017).

Recent research by Zkhiri *et al.* (2018) extended this understanding by demonstrating increased drought in mountainous areas of the Tensift basin, which extends to all Moroccan mountains, impacting vegetation and downstream water resources in the plain. Similarly, Ouatiki *et al.* (2019) obtained comparable results in the Oum Er-Rbia basin adjacent to our study area. According to their study, the North Atlantic Oscillation (NAO) and the Atlas Mountain chain are major factors in the basin's significant year-to-year rainfall variability. Furthermore, it notes the prevalence of deficit years and a severe and long-lasting dry period during the 1980s (Ouatiki *et al.* 2019).

3.2. Trend analysis

From 1980 to 2018, we conducted an annual and seasonal trend analysis of the SPI index in the MS region at a significance level of 5%.

The annual-scale analysis showed no significant negative trends at approximately half of the stations, indicating a potential decrease in mean annual precipitation over time. Conversely, the other half of the stations exhibited no significant positive trends, suggesting an increase in mean annual rainfall. However, none of these trends reached statistical significance, highlighting the complexity of yearly precipitation variations. This lack of statistical significance implies that these trends may

Table 5 | Frequency analysis of SPI drought categories (%)

	Drought				Wet		
Station	Extreme	Severe	Moderate	Near Normal	Extreme	Severe	Moderate
Abadla	1.31	3.72	9.85	65.86	3.06	5.03	11.16
Adamna	4.81	4.60	4.60	69.80	0.88	4.60	10.72
Aghbalou	0.00	0.66	7.00	71.77	1.53	6.35	12.69
Benguerir	2.72	3.26	5.98	66.30	1.36	5.43	14.95
Bouchane	0.69	6.57	11.07	60.55	0.00	7.27	13.84
Chichaoua	1.10	3.97	12.14	64.46	2.21	6.40	9.71
Dyke of Safi	2.92	4.04	9.44	71.01	3.37	4.04	5.17
El Massira Dam	0.26	5.54	13.19	62.80	2.64	2.64	12.93
Iloudjane	0.59	5.87	8.21	67.45	2.64	6.74	8.50
Imin-Elhammam	0.00	4.60	10.28	66.08	3.94	5.91	9.19
Marrakech	1.75	5.91	9.19	66.30	3.06	7.00	6.78
Nkouris	1.31	8.32	9.85	67.61	3.50	2.63	6.78
Sidi Bou-Othman	0.59	7.04	7.62	67.45	2.64	5.28	9.38
Sidi Rahal	1.97	1.09	8.75	65.65	2.19	7.44	12.91
Skhor Rhamna	1.18	7.10	7.10	68.93	1.18	6.80	7.69
Taferiat	3.13	0.78	10.18	69.71	0.52	4.18	11.49
Tahanaout	1.09	6.35	8.10	68.49	3.72	5.47	6.78
Talmest	4.11	3.52	8.80	65.10	0.88	3.52	14.08

result from random fluctuations rather than systematic climate change. Nevertheless, it underscores the need for more comprehensive analysis with available data.

When analyzing the data analysis at a seasonal scale, we found no significant downward trends in half of the region's stations (9 out of 18 stations) during the winter period (December, January, and February), aligning with the annual findings. The other half of the stations displayed no significant upward trends, indicating potential shifts in winter precipitation patterns. However, the absence of statistical significance suggests that these changes are not firmly linked to systematic climate shifts. Contributing factors may include natural climate fluctuations, geographic influences, and local weather patterns.

In spring (March, April, and May), the majority of stations (78%) showed no significant negative trends (Figure 6 and Table 6). Three stations (Bouchane, Nkouris, and Sidi Bou-Othman) displayed no significant positive SPI trends, and the dyke of Safi station exhibited a significant positive trend (p-value = 0.042), aligning with previous studies (Knippertz *et al.* 2003; Ouatiki *et al.* 2019; Hadri *et al.* 2021a). These results indicate a decline in spring precipitation trends in northwest Africa, reflecting a global trend toward drier circumstances.

During the summer (June, July, and August), 9 of the 18 stations showed no significant downward trends, while 8 stations displayed no significant upward trends. The Nkouris station had a significant upward trend (p-value = 0.014), consistent with findings in Diani *et al.* (2019), Hadria *et al.* (2019), and Ouatiki *et al.* (2019). These trends can be attributed to extreme summer rainfall events, such as showers, contributing to flash floods.

In autumn (September, October, and November), four stations (Aghbalou, Dyke of Safi, Marrakech, and Sidi Rahal) exhibited significant positive trends. Most other stations in the MS region showed positive trends, although not statistically significant. The Benguerir station displayed a no-significant negative trend, suggesting an overall positive trend in the region with some local fluctuations. These observations confirm an increase in autumn rainfall values, consistent with prior research (Caloiero *et al.* 2018; Domínguez-Castro *et al.* 2019).

The results of our study are in line with previous research conducted in Morocco. Hadri *et al.* (2021a) studied Chichaoua-Mejjate from 1970 to 2017, and Hadria *et al.* (2019) covered Morocco from 1998 to 2012. The MK test indicated mixed trends in both cases, none of which were statistically significant. These trends included negative trends in winter and spring and

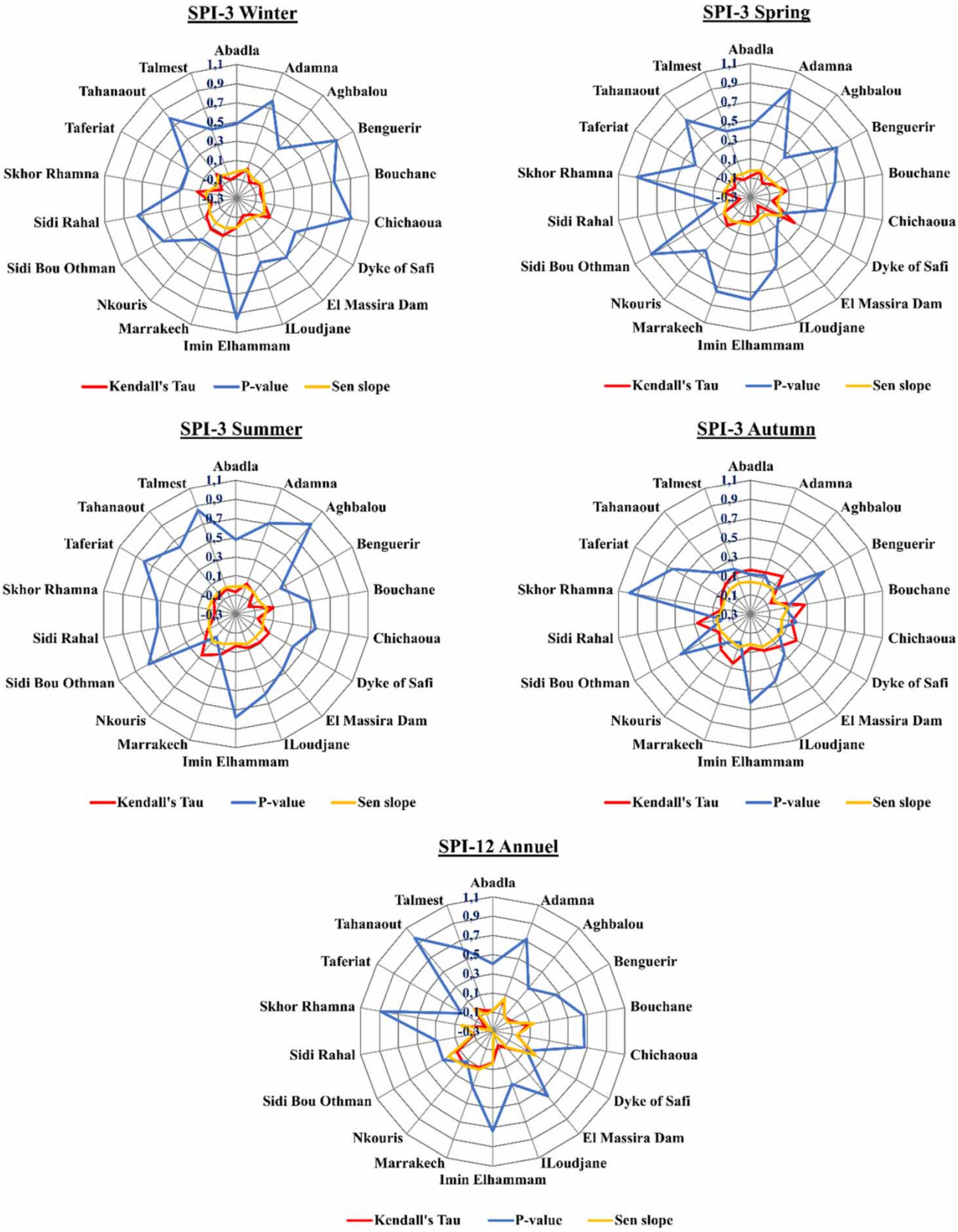

Figure 6 | Radar graph of MK test results for SPI at various time intervals.

Table 6 | MK test results of the SPI calculated in different time scales

	SPI3_Winter			SPI3_Spring			SPI3_Summer			SPI3_Autumn			SPI12_Annuel		
Stations	**Kendall's Tau**	***P*-value**	**Sen slope**	**Kendall's Tau**	***P*-value**	**Sen slope**	**Kendall's Tau**	***P*-value**	**Sen slope**	**Kendall's Tau**	***P*-value**	**Sen slope**	**Kendall's Tau**	***P*-value**	**Sen slope**
Abadla	−0.071	0.474	−0.019	−0.078	0.433	−0.021	−0.072	0.474	−0.014	0.157	0.113	0.037	−0.083	0.403	−0.087
Adamna	0.032	0.779	0.014	−0.016	0.893	−0.006	0.042	0.711	0.008	0.164	0.135	0.04	0.039	0.728	0.059
Aghbalou	−0.087	0.384	−0.028	−0.117	0.238	−0.033	−0.01	0.924	−0.004	**0.214**	**0.03**	**0.058**	−0.107	0.281	−0.102
Benguerir	−0.014	0.907	−0.003	−0.039	0.735	−0.011	−0.139	0.241	−0.026	−0.064	0.58	−0.02	−0.089	0.46	−0.119
Bouchane	−0.053	0.726	−0.02	0.08	0.591	0.036	0.104	0.483	0.033	0.267	0.065	0.096	0.067	0.657	0.138
Chichaoua	−0.012	0.912	−0.006	−0.072	0.48	−0.023	−0.062	0.545	−0.007	0.134	0.187	0.027	−0.043	0.673	−0.051
Dyke of Safi	0.093	0.411	0.027	**0.228**	**0.042**	**0.075**	0.099	0.384	0.023	**0.244**	**0.029**	**0.073**	0.179	0.11	0.216
El Massira Dam	−0.083	0.505	−0.035	−0.19	0.125	−0.064	0.091	0.466	0.02	0.147	0.243	0.056	−0.068	0.588	−0.075
ILoudjane	−0.108	0.412	−0.05	−0.099	0.464	−0.045	0.072	0.599	0.036	0.101	0.443	0.06	−0.143	0.285	−0.276
Imin-Elhammam	0.005	0.965	0.003	−0.031	0.769	−0.011	0.03	0.776	0.006	0.049	0.631	0.016	0.034	0.741	0.039
Marrakech	0.113	0.278	0.033	−0.034	0.754	−0.013	0.142	0.178	0.033	**0.248**	**0.017**	**0.066**	0.106	0.317	0.122
Nkouris	0.116	0.265	0.039	0.084	0.43	0.026	**0.257**	**0.014**	**0.07**	0.179	0.085	0.045	0.163	0.122	0.164
Sidi Bou-Othman	0.071	0.592	0.027	0.02	0.896	0.022	0.044	0.75	0.017	0.08	0.544	0.055	0.138	0.302	0.236
Sidi Rahal	−0.031	0.756	−0.007	−0.188	0.061	−0.051	−0.064	0.528	−0.018	**0.267**	**0.007**	**0.061**	−0.106	0.29	−0.091
Skhor Rhamna	0.118	0.289	0.034	−0.014	0.907	−0.003	−0.074	0.539	−0.01	0.003	0.99	0.001	0.018	0.887	0.03
Taferiat	−0.126	0.293	−0.05	−0.111	0.366	−0.038	−0.032	0.804	−0.016	0.057	0.646	0.016	−0.214	0.078	−0.286
Tahanaout	0.027	0.797	0.003	−0.032	0.755	−0.009	−0.051	0.612	−0.016	0.113	0.259	0.036	0.005	0.971	0.002
Talmest	−0.093	0.466	−0.033	−0.103	0.432	−0.045	−0.026	0.851	−0.003	0.164	0.202	0.048	−0.067	0.61	−0.112

All values in bold indicate a trend.

positive trends in autumn and summer. The occasional positive trends in the SPI noted by Hadria *et al.* (2019) and Hadri *et al.* (2021a) were attributed to localized intense rainfall events. Conversely, during drought periods, deviations from the average were more noticeable. Our analysis supported these findings, with no significant SPI drought index trends, except for the extreme eastern and southern regions of Morocco, aligning with Hadria *et al.* (2019) observations. These results are consistent with other Moroccan studies (Khomsi *et al.* 2016; Boughdadi *et al.* 2023) and global climate trends. Recent research (Barcikowska *et al.* 2018; Wang *et al.* 2018) has suggested that climate change may be altering large-scale flow patterns, significantly impacting the Mediterranean hydroclimate.

Several authors (Vicente-Serrano *et al.* 2011; Caloiero *et al.* 2018) attribute the occurrence of drought events to the NAO and its impact on global precipitation. NAO, a recurring atmospheric and oceanic phenomenon, plays a pivotal role in shaping climate variability across a vast geographic expanse, from the United States East Coast to Siberia and the subtropical Atlantic (Hurrell *et al.* 2003; Niazi 2007). Positive NAO phases induce winter and autumn droughts in southern Europe and northwest Africa, while negative NAO phases are linked to deficits in northern and Near East Africa. The transition to drier conditions in the region signifies global warming and is associated with changes in atmospheric patterns, particularly a reduction in northern disturbances during winter and spring (Ait Brahim *et al.* 2017; Boughdadi *et al.* 2023).

3.3. Spatial and temporal comparison of drought indices by remote sensing

The VCI, TCI, and VHI indices were calculated and mapped for each month (March, June, and December) from 2000 to 2018, using normalized difference vegetation index (NDVI) and land surface temperature (LST) data generated by the TERRA/AQUA satellite with its MODIS sensor in the MS region. The indices mentioned above facilitate the categorization of drought into five categories: extreme, severe, moderate, mild, and no drought.

In the context of this study, the months of March, June, and December were chosen to evaluate the impact of humidity and heat stress on vegetation for several reasons. March is considered the beginning of spring, a crucial period for crop development, as early precipitation is essential for growth. June is characterized by intensive water resource usage, particularly groundwater, for crop irrigation. December is regarded as a critical month for seasonal and winter crops.

The results of the VCI, TCI, and VHI indices for March from 2000 to 2018 are depicted in Figures 7 and 8. In 2001, the VCI indicated severe and moderate drought, with the same percentage for each class representing 27.59% of the total area, while the coastal zone experienced no drought. The TCI indicated that the region experienced extreme to severe drought, accounting for 86.82% of the total area, while the VHI revealed a similar extent of extreme to severe drought, representing 69.66% of the entire area. In 2002, the VCI showed extreme to moderate drought, with percentages of 34.20, 25.14, and 15.25%, respectively. The TCI and VHI reflected a very wet year, with percentages of 97.59 and 74.55%, respectively. From 2003 to 2004, the subsequent years were characterized by wet conditions according to the VCI, TCI, and VHI indices. In 2005, the VCI exhibited extreme to severe drought, affecting 42.92% of the study area. The TCI indicated no drought, with a percentage of 60.87%, while the VHI revealed moderate to mild drought in the central region. In 2006, the VCI, TCI, and VHI indices indicated wet conditions, with percentages of 91.04, 74.08, and 86.46%, respectively. The years 2007–2008 witnessed a significant return to drought, with high percentages of severe to extreme drought according to all three indices. From 2009 to 2010, very wet conditions prevailed across the region, with percentages exceeding 90% of the total study area. In 2011, moderate drought persisted in the lowland zone. In 2012, drought returned significantly throughout the region, with high percentages of severe and moderate drought according to all three indices. From 2013 to 2014, moderate drought persisted, although slightly less pronounced than in previous years. In 2015, a significant decrease in drought was observed, with high percentages of nondrought. In 2016, extreme drought was more pronounced than in previous years, with a percentage of 57%, according to the VCI. However, moderate to mild drought remained dominant, according to the TCI and VHI. From 2017 to 2018, drought conditions varied yearly and regionally, but mild to moderate drought persisted according to the VCI, TCI, and VHI.

The results of the VCI, TCI, and VHI indices for June from 2000 to 2018 are shown in Figures 9 and 10. Regarding the VCI, the MS region experienced significant levels of vegetation stress, with extreme to severe drought covering almost the entire region. Exceptionally high percentages were observed in the following years: 2000, 2001, 2005, 2007, and 2008, with percentages of extreme to severe drought reaching 57.37, 80.46, 58.73, 63.1, and 75.12%, respectively. Furthermore, there were extremely wet conditions in 2004, 2006, 2009, 2010, 2011, 2015, and 2018, with drought percentages below 20%. In terms of the TCI, some years, they have exhibited drier conditions with high percentages of moderate to extreme drought, while other years showed lower levels of drought, with higher percentages indicating no drought. Years such as 2000, 2001,

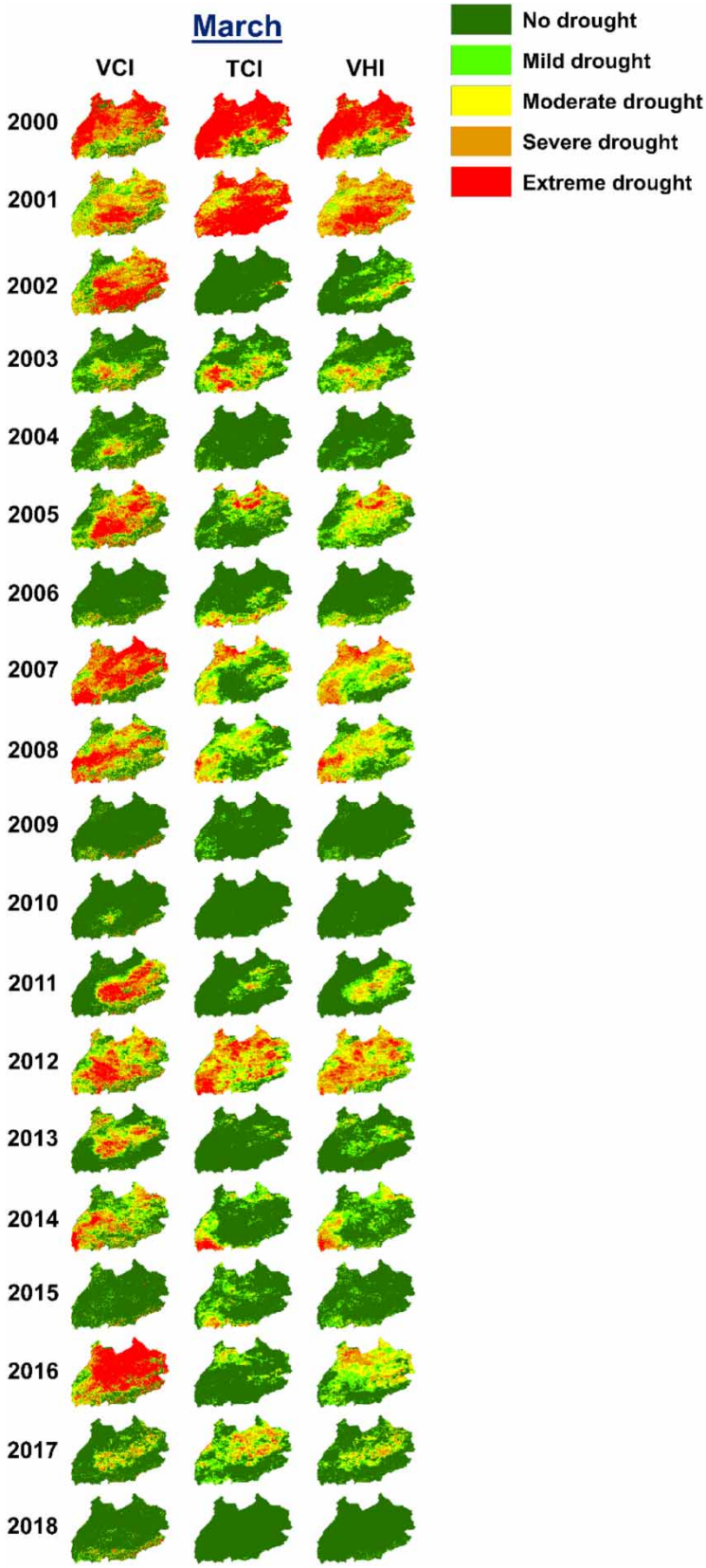

Figure 7 | Maps of the Marrakech-Safi region's VCI, TCI, and VHI from 2000 to 2018 in March.

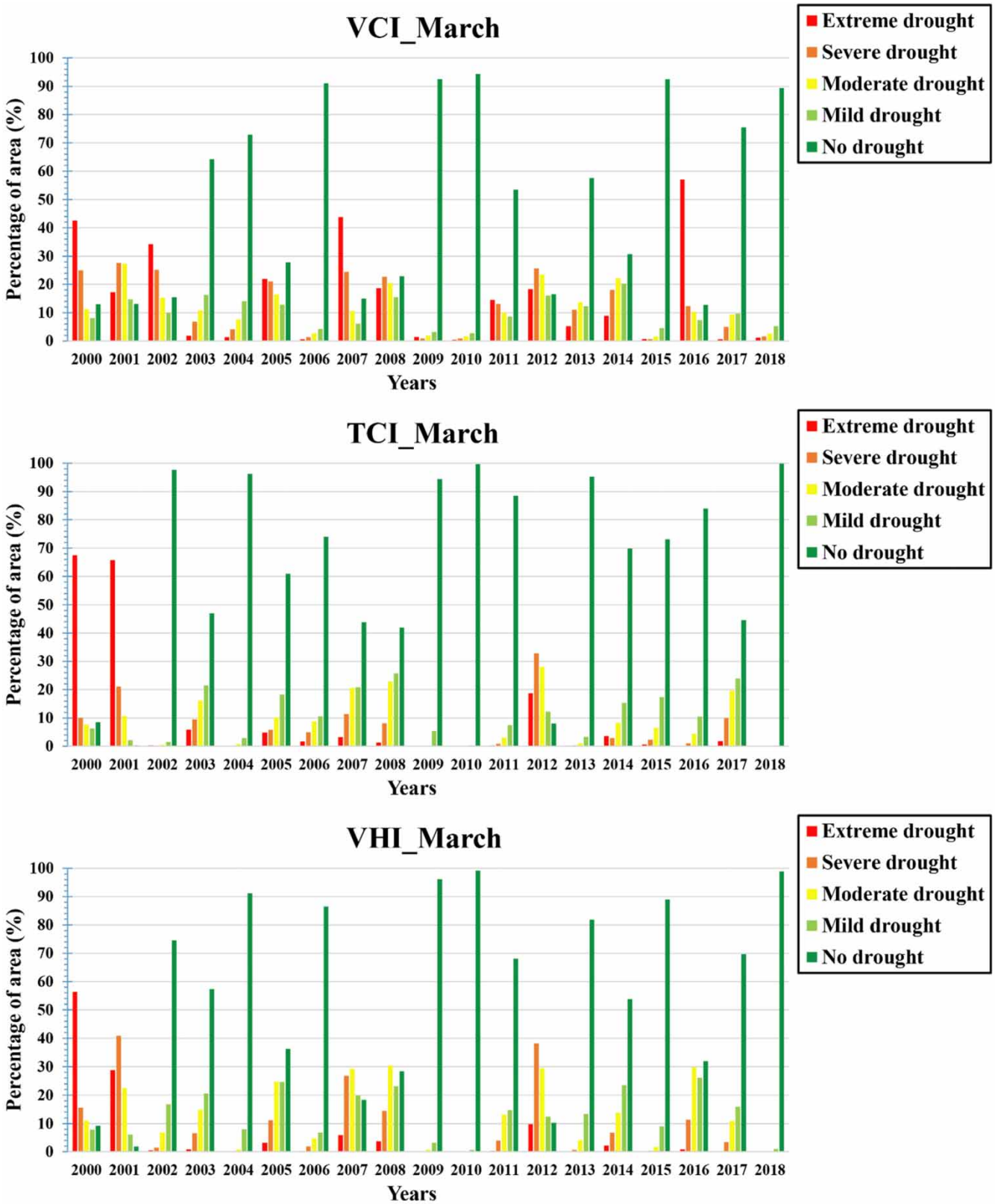

Figure 8 | Spatial-temporal assessment of VCI, TCI, and VHI from 2000 to 2018 in March.

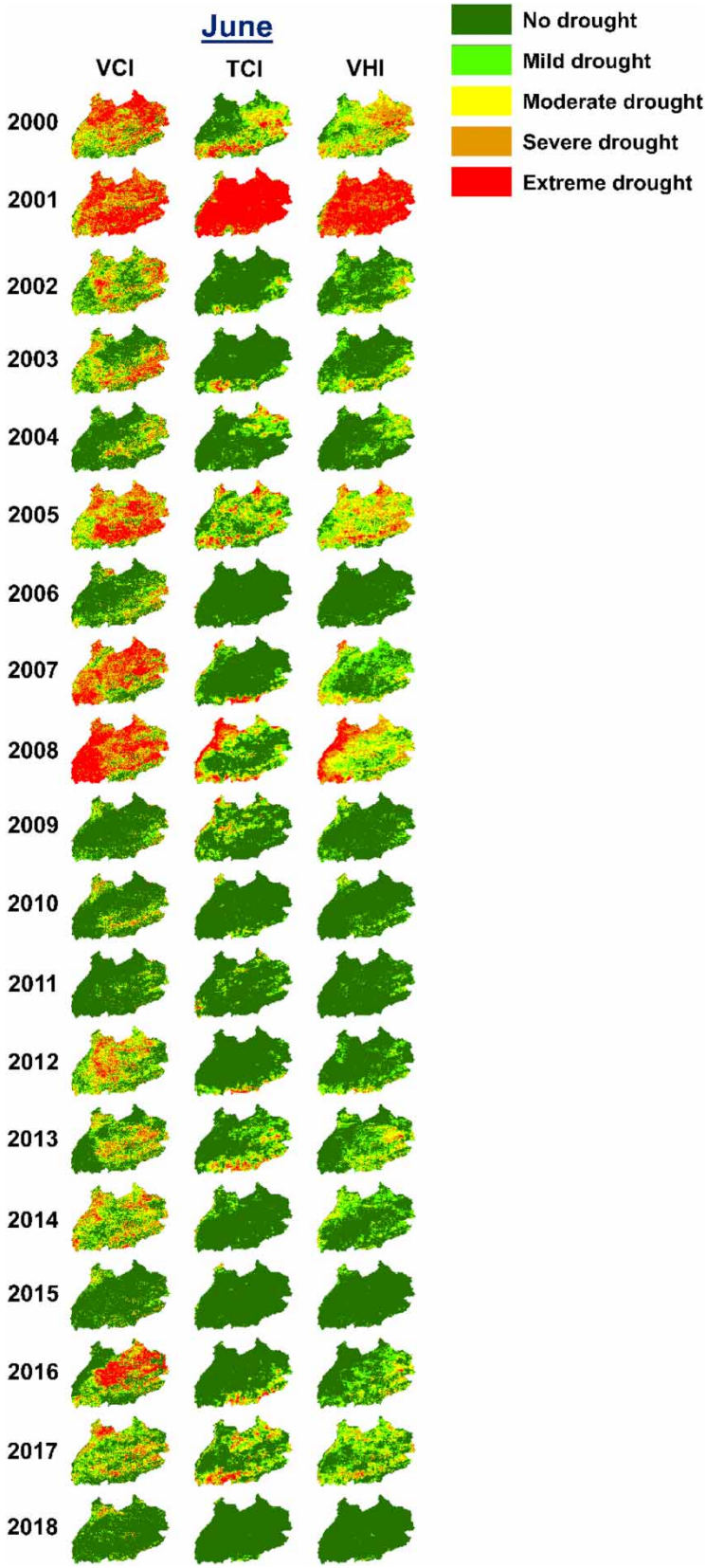

Figure 9 | Maps of VCI, TCI, and VHI of the Marrakech-Safi region during the period 2000–2018 in June.

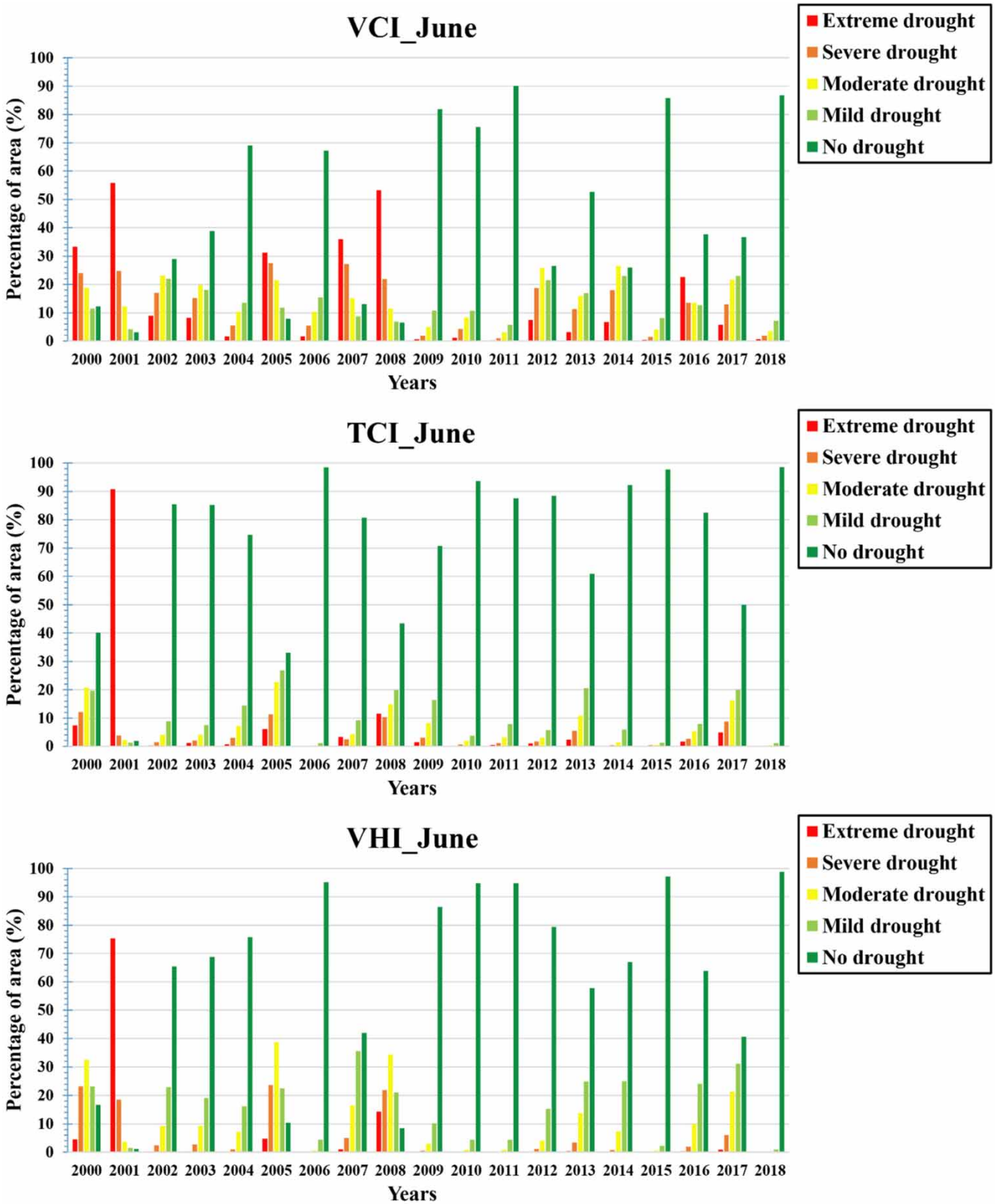

Figure 10 | Spatial-temporal assessment of VCI, TCI, and VHI in June from 2000 to 2018.

2005, and 2008 were distinguished by relatively low 'no drought' percentages and a predominance of mild to extreme drought, suggesting high temperatures and limited water availability for vegetation. In contrast, years with wet conditions, such as 2002, 2003, 2006, 2007, 2010, 2011, 2012, 2014, 2015, 2016, and 2018, showed percentages over 80%, indicating no drought, suggesting lower temperatures and higher precipitation levels during this period. The VHI revealed that plant health was more negatively affected, especially in the years 2000 (83.40%), 2001 (98.92%), 2005 (89.59%), 2007 (58.03%), 2008 (91.52%), and 2017 (60%). This finding can be attributed to the extensive exposure of the region to extreme and severe drought conditions.

The results of the VCI, TCI, and VHI indices for December between 2000 and 2018 have been illustrated in Figures 11 and 12. It is important to note that the MS region experienced significant drought during this period. The years 2000, 2001, and 2015 stand out as periods of extreme drought, with a high percentage of 67.15, 81.86, and 84.22% in this category, respectively. Other years, such as 2009, 2010, 2011, 2013, and 2017, were also characterized by severe to moderate drought. This finding indicates severe drought conditions and potentially devastating consequences for agriculture and water resources. In contrast, the years 2003 and 2012 showed an improvement in the situation, with a lower percentage of extreme drought, accounting for less than 1.25% of the total surface area of the study area.

Compared to Hanadé Houmma *et al.*'s (2022) findings, our study confirms fluctuating drought conditions in the MS region, specifically in the Tensift basin. This region faces significant challenges related to agriculture and water resources, with extreme drought conditions occurring in nearly half of the Tensift basin areas in 2005, 2008, 2012, 2016, and 2020, highlighting irregular alternations among dry, wet, and normal years.

Our results align with previous studies by Amalo *et al.* (2017) and Wyss *et al.* (2022), emphasizing the significance of remote sensing-based drought indices for identifying and monitoring drought events. Wang *et al.* (2014) have also provided evidence of successful applications in places like China.

Additionally, remote sensing indicators have been confirmed as effective tools for drought monitoring in various Moroccan regions, such as the Doukkala region (Ait Ayad *et al.* 2023), Souss-Massa region (Mounir *et al.* 2023), and the Moulouya and Tensift watersheds (Hanadé Houmma *et al.* 2022). These indices, including the VCI, TCI, and VHI, consistently demonstrate their value, efficiency, and cost-effectiveness in this context. VCI serves as a reliable tool for identifying drought start and duration, although it may misinterpret uninhabited land post-harvest. TCI effectively tracks drought in Morocco regions and detects stress brought on by high temperatures or humidity. VHI provides a better comprehension of drought occurrences.

3.4. Monthly correlations between remote sensing-based drought indices and multi-scale SPI

Figures 13 and 14 provide a visual representation of the spatial distribution of Pearson correlation and the mean Pearson correlation coefficients (R) calculated between the drought indices derived from satellite data (VCI and VHI) and the drought index derived from rainfall data (SPI). These calculations were performed at various time scales of 3, 6, and 12 months, focusing on the period from 2000 to 2018, specifically for the months of March, June, and December.

The correlation analysis revealed significant findings regarding the relationship between different drought indices and vegetation conditions in various regions and time scales. In March, the monthly VCI exhibited a significant positive correlation with SPI-3 months, SPI-6 months, and SPI-12 months in the plateau, plain, Jebilet chain, and Chichaoua-Essaouira basin zones. The mean correlation coefficients (R) for these relationships were 0.56, 0.60, and 0.53, respectively, representing the entire study area. In contrast, a weak correlation was observed in the High Atlas region. Similar results were obtained for the correlation between monthly VHI and SPI (3, 6, and 12 months), except for the absence of correlation between VHI and SPI-12 months in the Essaouira region. These findings indicate a close link between vegetation conditions and rainfall variations across different time scales. During June, a strong correlation was observed between VCI and SPI (6 and 12 months) throughout the region, with the mean correlation coefficients (R) of 0.59 and 0.61, respectively. However, a weak correlation was found between VCI and SPI-3 months ($R = 0.28$), suggesting that other factors or time scales may influence vegetation conditions during this period. Similar results were observed for VHI.

In December, the correlation between VCI and SPI (3, 6, and 12 months) was moderate to low in the central region and the High Atlas, while it was strong in the rest of the area. Similar results were observed for VHI. This analysis indicates that the SPI-6 months are more relevant for assessing vegetation activity in the MS region during the least examined months (March, June, and December). Additionally, the SPI-12 months produced similar results in March and June, emphasizing the importance of this time scale in assessing the impact of drought on vegetation activity. These findings highlight the significance of considering multiple time scales to comprehensively understand the climatic influence on vegetation.

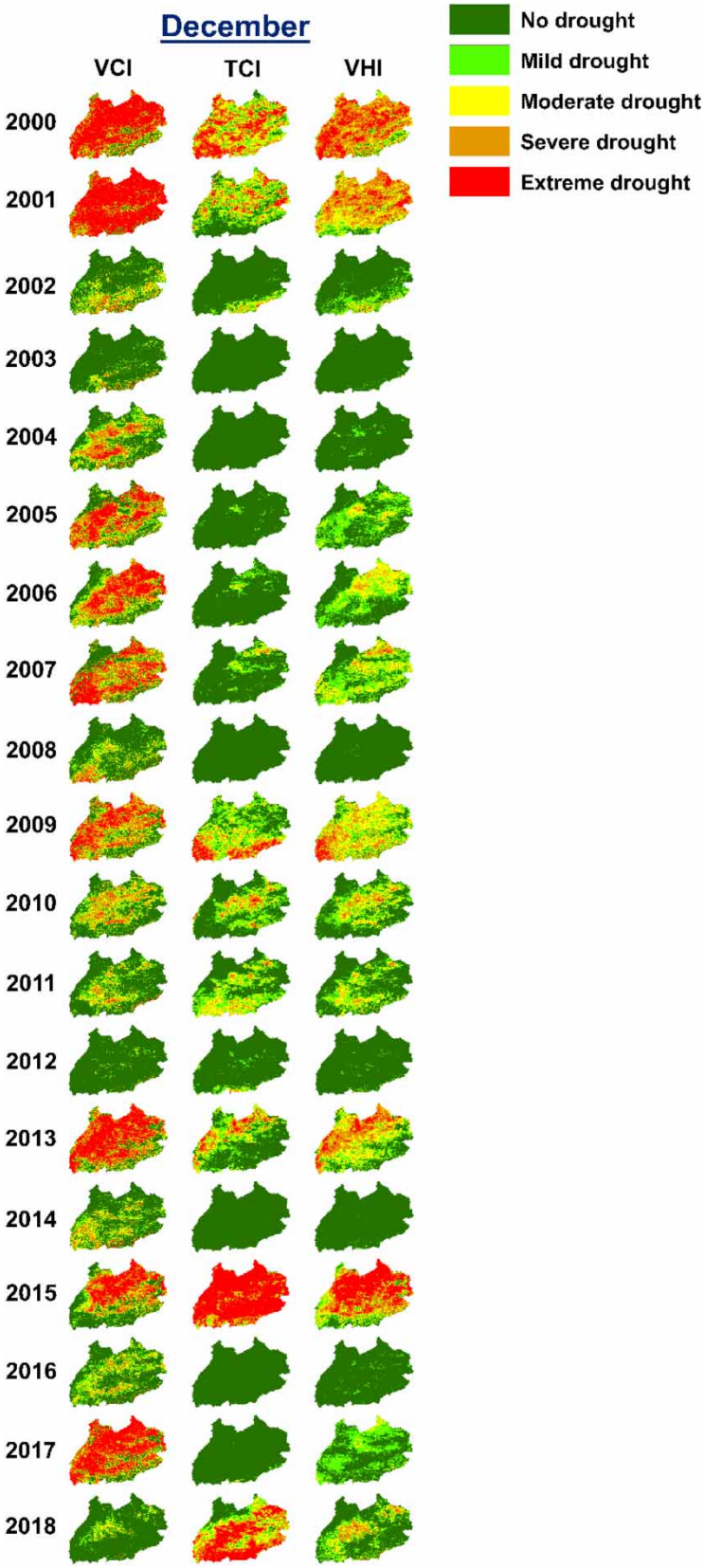

Figure 11 | Maps of VCI, TCI, and VHI of the Marrakech-Safi region from 2000 to 2018 in December.

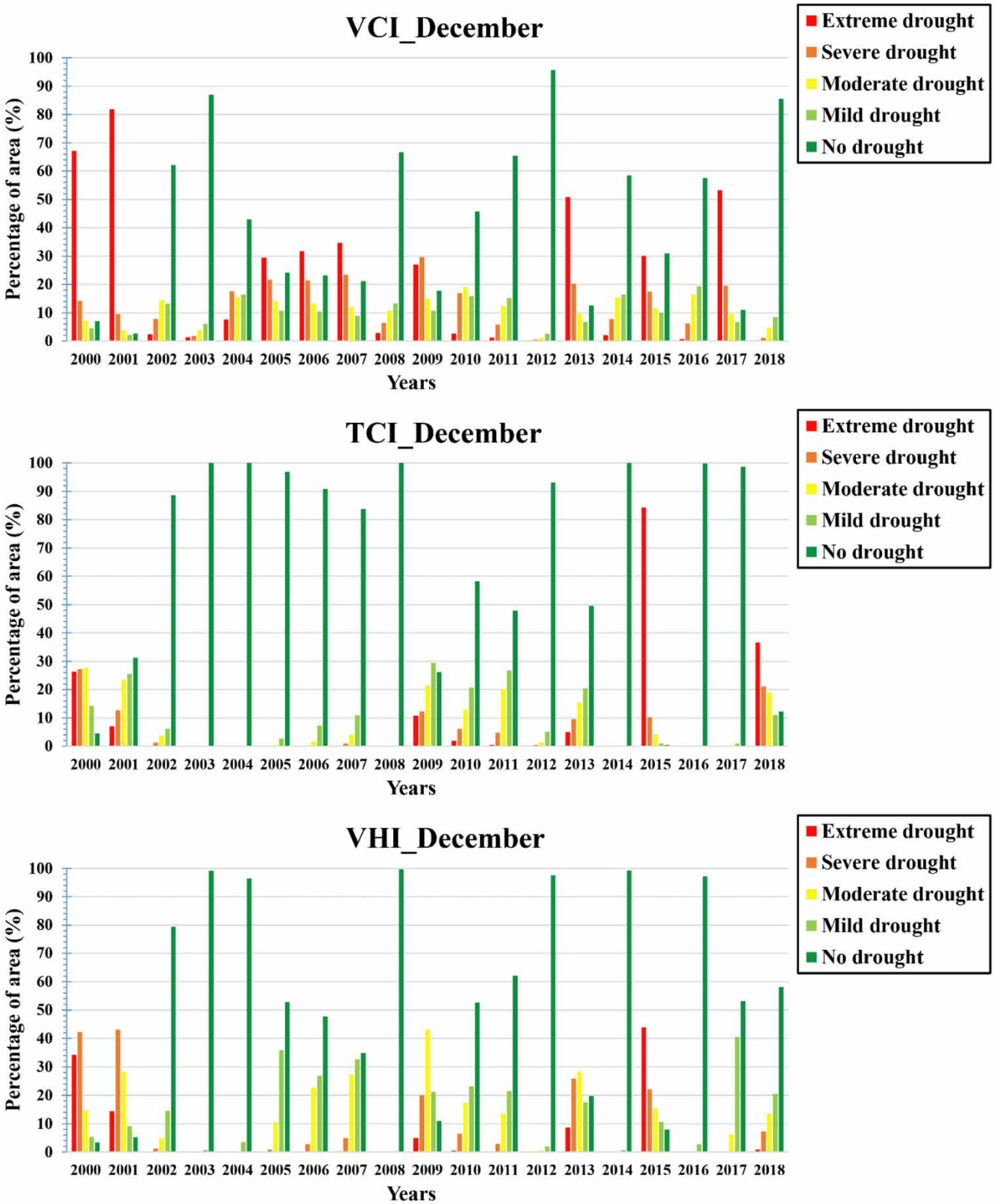

Figure 12 | Spatial-temporal assessment of VCI, TCI, and VHI from December 2000 to 2018.

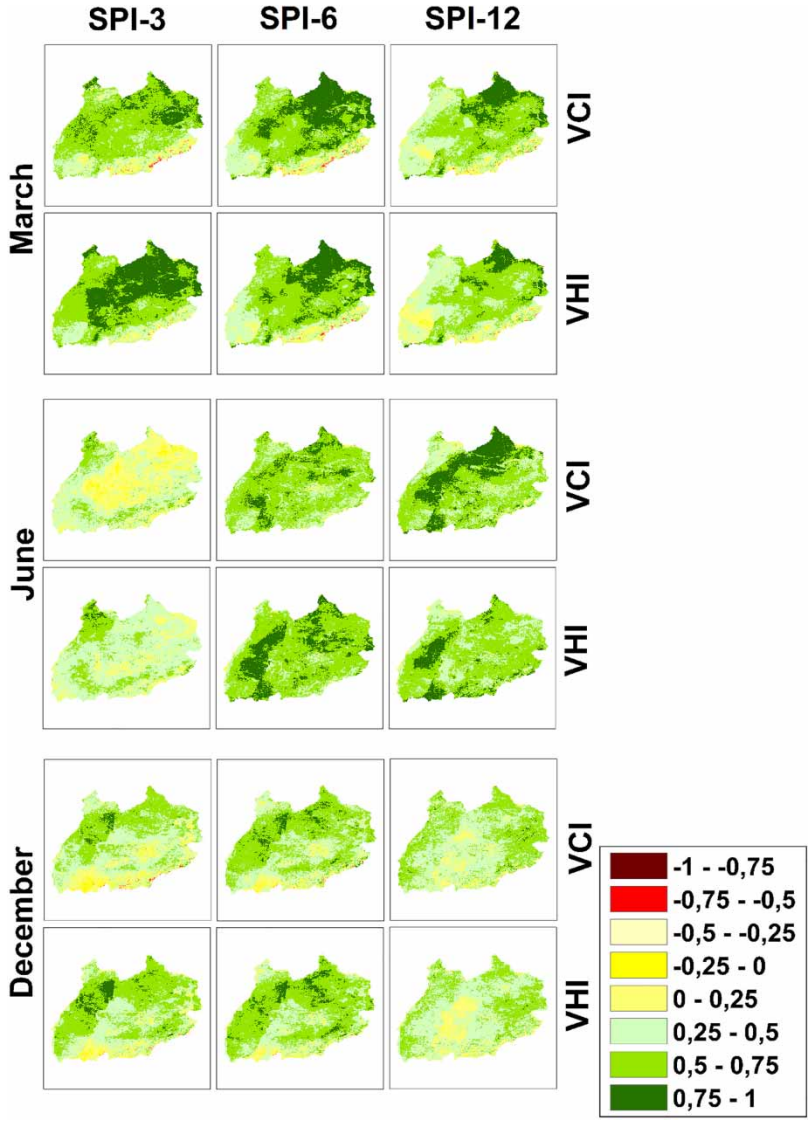

Figure 13 | Spatial distribution of Pearson's correlation coefficient between VCI, VHI, and multi-scale SPI in the study area.

Table 7 presents the percentage of the total area with positive and negative correlations between drought indices in the study area over the 3 months (March, June, and December). The correlation value R indicates the level of correlation between SPI (3, 6, and 12 months) and VCI, as well as VHI. A value of $R > 0.5$ indicates a strong positive correlation, $0 < R < 0.5$ indicates a weak positive correlation, $-0.5 < R < 0$ indicates weak or no correlation, and $R < -0.5$ indicates a strong negative correlation. The results demonstrate that correlations vary based on the drought index, time scale, and month.

In March, 73% of the total area exhibited a positive correlation between SPI-3 months and VCI, while 24% displayed a negative correlation. For June, 78% of the total area showed a positive correlation between SPI-6 months and VCI, while 22% exhibited a negative correlation. In December, 42% of the total area displayed a positive correlation between SPI-12 months and VCI, while 57% showed a negative correlation. Similar patterns were observed for VHI. These findings suggest that SPI-6 months could be a reliable tool for mapping and monitoring agricultural drought conditions due to its sensitivity to vegetation conditions. Furthermore, it can be concluded that the precipitation accumulations recorded during the previous 6 months have the most critical impact on vegetation activity.

This study demonstrates a strong correlation between the interannual variability of drought and vegetation activity in the MS region using a variety of remote sensing and meteorological indices. In June, statistically significant positive correlations were observed between SPI6-VCI, SPI6-VHI, SPI12-VCI, and SPI12-VHI in over 75% of the study area.

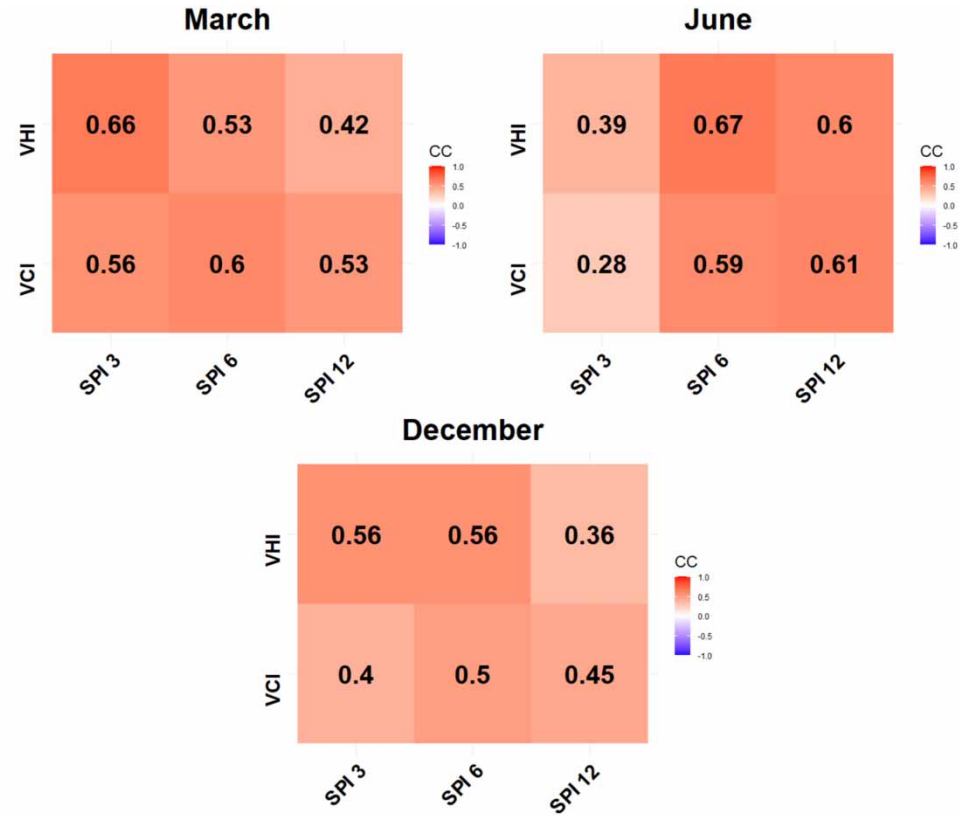

Figure 14 | Heatmap of mean Pearson correlation coefficients (*R*) among SPI, VCI, and VHI drought indices (March, June, December).

Table 7 | Percentage of the total area showing positive and negative correlations of drought indices in the Marrakech-Safi region

		VCI				VHI			
		Positive *R* > 0.5	**Positive *R* < 0.5**	**|Negative| *R* < 0.5**	**|Negative| *R* > 0.5**	**Positive *R* > 0.5**	**Positive *R* < 0.5**	**|Negative| *R* < 0.5**	**|Negative| *R* > 0.5**
SPI 3	*March*	**73%**	24%	3%	0%	**83%**	16%	1%	0%
	June	14%	**79%**	7%	0%	22%	**78%**	0%	0%
	December	38%	**56%**	5%	0%	**69%**	30%	1%	0%
SPI 6	*March*	**74%**	24%	2%	0%	**66%**	32%	2%	0%
	June	**78%**	22%	1%	0%	**90%**	9%	0%	0%
	December	**58%**	39%	3%	0%	**69%**	30%	1%	0%
SPI 12	*March*	**61%**	36%	3%	0%	40%	**57%**	3%	0%
	June	**75%**	24%	1%	0%	**79%**	21%	0%	0%
	December	42%	**57%**	1%	0%	20%	**78%**	2%	0%

This highlights the highest percentages of the total area exhibiting both positive and negative correlations of drought indices.

The findings are consistent with prior research that highlights a significant correlation between drought indices derived from remote sensing (VCI and VHI) and SPI across different temporal scales. In Ethiopia, Senamaw *et al.* (2021) substantiated a strong correlation between SPI and VCI, specifically during the crop-growing season. Similarly, Wang *et al.* (2014) illustrated a persistent association between SPI and VHI in southwestern China, providing insights into vegetation resilience during drought. Javed *et al.* (2020) observed robust Pearson correlation results in China, underscoring the necessity of examining diverse time scales. They particularly emphasized the correlation of VCI with SPI3 for cropland and SPI6 for forests.

Our research shows that in certain areas like plains, plateaus, foothills, and near the coast, there are strong and meaningful connections between different measures of drought and vegetation health in March. However, in the mountainous region,

these are not as clear. Hadri *et al.* (2021a) explain that the types of land, how we use the land for farming, and the quality of irrigated land all play a role in how these connections change throughout the year. We noticed that in places where farmers rely on rain for their crops, like barley and grains, we see a significant impact during the spring when drought is more common. In areas where farmers irrigate their crops, the connection is not strong, possibly because they use more groundwater after March, regardless of how much it actually rains. This creates some challenges when using remote sensing to monitor drought, as highlighted in studies by Ezzine *et al.* (2014) and Hadri *et al.* (2021a).

In the mountainous areas, which are high and have a relatively wet climate, we found weaker connections between SPI and drought indices derived from remote sensing. This is because the plants in these areas, such as forests, dry pastures, and shrubs, are adapted to the local climate. Despite drought conditions being documented, the vegetation here can still get water from deep in the soil. Studies by Herrmann *et al.* (2016) and Hadri *et al.* (2021a) consistently show that vegetation in areas with more moisture is less affected by drought compared to dry environments.

4. CONCLUSION

Drought is one of the most complex natural disasters, with severe consequences worldwide. It has adverse effects, such as reducing water supply to urban and rural areas, crop yields, industrial production, and hydroelectric power generation. Moreover, droughts cannot be avoided, but their impacts can be reduced through comprehensive risk management strategies based on planning, mitigation, monitoring, early warning, and forecasting.

This paper aims to characterize meteorological drought's spatial and temporal pattern using the SPI index from 1980 to 2018. Additionally, it investigates agricultural drought in March, June, and December in MS during the period 2000–2018, using the VCI, TCI, and VHI indices. The analysis and interpretation of the results have led to various conclusions, which are further elaborated upon based on specific objectives. These findings demonstrate that all drought-prone areas experienced different types of droughts, ranging from mild to extreme, over an extended period. It is important to note that most previous studies have focused on specific regions without including the MS region.

The results of this study lead to the following conclusions:

i. The study of drought on different time scales in the MS region utilizes the SPI to identify drought and wet episodes in the region's 18 rainfall stations from 1980 to 2018, based on the SPI-12 index. Evaluating the results reveals alternating periods of severe to extreme drought with rainfall deficits and wet to extremely wet periods with rainfall surpluses.
ii. The MK test assessed drought trends in the MS region from 1980 to 2018. Analyzing the SPI index for annual and seasonal variations, we identified specific stations with no significant downward trends, indicating a decrease in mean annual precipitation. However, other stations showed no significant upward trends. Seasonally, spring and winter displayed no significant negative trends, whereas autumn and summer exhibited significant upward trends.
iii. The analysis of the VCI, TCI, and VHI indices, based on NDVI and LST satellites from 2000 to 2018, reveals a significant spatio-temporal variability in droughts, ranging from extreme to severe, as well as wet periods in the MS region. The years 2000, 2001, 2007, and 2012 witnessed extreme to severe drought conditions, whereas extremely wet conditions characterized 2010, 2015, and 2018.
iv. Although data on drought in the MS region are limited, satellite drought indices, such as VCI, TCI, and VHI, have proven to be a suitable approach for predicting agricultural drought's spatial and temporal distribution on a pixel-by-pixel basis. They have also been instrumental in developing adaptation techniques to mitigate drought damage in our study region.
v. The analysis of the correlation between VCI, VHI, and SPI for different periods (3, 6, and 12 months) and months (March, June, and December) reveals a positive correlation between these indices, suggesting a significant relationship between vegetation health, precipitation, and temperature.

These results will allow other researchers and local stakeholders to understand better and identify risks and vulnerabilities concerning dry and wet episodes. This knowledge will benefit water resource management, sustainable development, information dissemination, protection, prevention, and risk forecasting in the MS region. Further research is required to establish a reliable scientific foundation for developing risk management strategies and monitoring tools. Enhancing the organization's capacity to adapt to present, future, and unforeseen drought and climate change challenges will be beneficial.

DATA AVAILABILITY STATEMENT

All relevant data are included in the paper or its Supplementary Information.

CONFLICT OF INTEREST

The authors declare there is no conflict.

REFERENCES

AghaKouchak, A., Farahmand, A., Melton, F. S., Teixeira, J., Anderson, M. C., Wardlow, B. D. & Hain, C. R. 2015 Remote sensing of drought: Progress, challenges and opportunities. *Reviews of Geophysics* **53** (2), 452–480. https://doi.org/10.1002/2014RG000456.

Ait Ayad, N., Ait Ayad, A., El Khalidi, K., Habib, A. & Charif, A. 2023 Remote sensing and meteorological indexes of drought using open short time-series data in Doukkala Region, Morocco. *Ecological Engineering & Environmental Technology* **24** (2), 1–10. https://doi.org/10.12912/27197050/156962.

Ait Brahim, Y., Saidi, M. E. M., Kouraiss, K., Sifeddine, A. & Bouchaou, L. 2017 Analysis of observed climate trends and high resolution scenarios for the 21st century in Morocco. *Journal of Materials and Environmental Science* **8** (4), 1375–1384.

Aksu, H., Cavus, Y., Aksoy, H., Akgul, M. A., Turker, S. & Eris, E. 2022a Spatiotemporal analysis of drought by CHIRPS precipitation estimates. *Theoretical and Applied Climatology* **148** (1–2), 517–529. https://doi.org/10.1007/s00704-022-03960-6.

Aksu, H., Cetin, M., Aksoy, H., Yaldiz, S. G., Yildirim, I. & Keklik, G. 2022b Spatial and temporal characterization of standard duration-maximum precipitation over Black Sea Region in Turkey. *Natural Hazards* **111** (3), 2379–2405. https://doi.org/10.1007/s11069-021-05141-6.

Almazroui, M., Saeed, F., Saeed, S., Nazrul Islam, M., Ismail, M., Klutse, N. A. B. & Siddiqui, M. H. 2020 Projected change in temperature and precipitation over Africa from CMIP6. *Earth Systems and Environment* **4** (3), 455–475. https://doi.org/10.1007/s41748-020-00161-x.

Alsenjar, O., Aksu, H. & Cetin, M. 2022 The Use of some specific drought indices to evaluate meteorological drought events in the Black Sea Region of Turkey. *Çukurova Tarım ve Gıda Bilimleri Dergisi* **37** (2), 261–272. https://doi.org/10.36846/CJAFS.2022.93.

Amalo, L. F., Hidayat, R. & Haris 2017 Comparison between remote-sensing-based drought indices in East Java. *IOP Conference Series: Earth and Environmental Science* **54** (1), 012009. https://doi.org/10.1088/1755-1315/54/1/012009.

Angelidis, P., Maris, F., Kotsovinos, N. & Hrissanthou, V. 2012 Computation of drought index SPI with alternative distribution functions. *Water Resources Management* **26** (9), 2453–2473. https://doi.org/10.1007/s11269-012-0026-0.

Ayugi, B., Eresanya, E. O., Onyango, A. O., Ogou, F. K., Okoro, E. C., Okoye, C. O., Anoruo, C. M., Dike, V. N., Ashiru, O. R., Daramola, M. T., Mumo, R. & Ongoma, V. 2022 Review of meteorological drought in Africa : Historical trends, impacts, mitigation measures, and prospects. *Pure and Applied Geophysics* **179** (4), 1365–1386. https://doi.org/10.1007/s00024-022-02988-z.

Barcikowska, M. J., Kapnick, S. B. & Feser, F. 2018 Impact of large-scale circulation changes in the North Atlantic sector on the current and future Mediterranean winter hydroclimate. *Climate Dynamics* **50** (5), 2039–2059. https://doi.org/10.1007/s00382-017-3735-5.

Barnes, W. L. & Salomonson, V. V. 1992 MODIS : A global imaging spectroradiometer for the Earth Observing System. *Optical Technologies for Aerospace Sensing: A Critical Review* **10269**, 280–302. https://doi.org/10.1117/12.161578.

Barnes, W. L., Xiong, X., Guenther, B. W. & Salomonson, V. 2003 Development, characterization, and performance of the EOS MODIS sensors. *Earth Observing Systems VIII* **5151**, 337–345. https://doi.org/10.1117/12.504818.

Bennani, O., Brahim, Y. A., Saidi, M. E. M. & Fniguire, F. 2016 Variability of surface water resources and extreme flows under climate change conditions in arid and mediterranean area : Case of Tensift watershed, Morocco. *Journal of Biodiversity and Environmental Sciences* **9** (4), 165.–174.

Bhuiyan, C. 2004 *Various Drought Indices for Monitoring Drought Condition in Aravalli Terrain of India*. 12–23.

Boughdadi, S., Ait Brahim, Y., El Alaoui El Fels, A. & Saidi, M. E. 2023 Rainfall variability and teleconnections with large-scale atmospheric circulation patterns in west-central Morocco. *Atmosphere* **14** (8), 1293. https://doi.org/10.3390/atmos14081293.

Bouras, E. H., Jarlan, L., Er-Raki, S., Albergel, C., Richard, B., Balaghi, R. & Khabba, S. 2020 Linkages between rainfed cereal production and agricultural drought through remote sensing indices and a land data assimilation system: A case study in Morocco. *Remote Sensing* **12** (24), 4018. https://doi.org/10.3390/rs12244018.

Bravo, R. Z. B., Cunha, A. P. M. d. A., Leiras, A. & Cyrino Oliveira, F. L. 2021 A new approach for a drought composite index. *Natural Hazards* **108** (1), 755–773. https://doi.org/10.1007/s11069-021-04704-x.

Caccamo, G., Chisholm, L. A., Bradstock, R. A. & Puotinen, M. L. 2011 Assessing the sensitivity of MODIS to monitor drought in high biomass ecosystems. *Remote Sensing of Environment* **115** (10), 2626–2639. https://doi.org/10.1016/j.rse.2011.05.018.

Caloiero, T., Caloiero, P. & Frustaci, F. 2018 Long-term precipitation trend analysis in Europe and in the Mediterranean basin: Long-term precipitation trend analysis. *Water and Environment Journal* **32** (3), 433–445. https://doi.org/10.1111/wej.12346.

CERED, & HCP 2017 *Projections de la population des régions et des provinces 2014*-2030. Haut-Commissariat au Plan. Available from: https://www.hcp.ma/region-drta/PROJECTIONS-DE-LA-POPULATION-DES-REGIONS-ET-DES-PROVINCES-2014–2030_a59.html.

Chang, S., Chen, H., Wu, B., Nasanbat, E., Yan, N. & Davdai, B. 2021 A practical satellite-derived vegetation drought index for arid and semi-arid grassland drought monitoring. *Remote Sensing* **13** (3), Article 3. https://doi.org/10.3390/rs13030414.

Dai, A. 2010 Drought under global warming : A review. *Wiley Interdisciplinary Reviews: Climate Change* **2** (1), 45–65. https://doi.org/10.1002/wcc.81.

Dai, A. 2011 Characteristics and trends in various forms of the Palmer drought severity index during 1900–2008. *Journal of Geophysical Research: Atmospheres* **116**, D12. https://doi.org/10.1029/2010JD015541.

Delserone, L. M. & Fleming, A. 2013 Reviews of science for science librarians: Drought in the agricultural and geosciences literature. *Science & Technology Libraries* **32** (1), 30–44. https://doi.org/10.1080/0194262X.2012.758551.

DGCL 2015 *La Monographie Générale de la région de Marrakech-Safi*. Ministère de l'intérieur, Direction Générale des Collectivités Locales. Available from: https://www.hcp.ma/region-marrakech/PRESENTATION-DE-LA-REGION-DE-MARRAKECH-SAFI_a248.html

Diani, K., Kacimi, I., Zemzami, M., Tabyaoui, H. & Haghighi, A. T. 2019 Evaluation of meteorological drought using the Standardized Precipitation Index (SPI) in the High Ziz River basin, Morocco. *Limnological Review* **19** (3), 125–135. https://doi.org/10.2478/limre-2019-0011.

Didan, K., Munoz, A. B. & Huete, A. 2015 *MODIS Vegetation Index User's Guide (MOD13 Series)*. University of Arizona: Vegetation Index and Phenology Lab, p. 35. Available from: https://modis-land.gsfc.nasa.gov/pdf/MOD13_User_Guide_V61.pdf

Domínguez-Castro, F., Vicente-Serrano, S. M., Tomás-Burguera, M., Peña-Gallardo, M., Beguería, S., El Kenawy, A., Luna, Y. & Morata, A. 2019 High spatial resolution climatology of drought events for Spain: 1961–2014. *International Journal of Climatology* **39** (13), 5046–5062. https://doi.org/10.1002/joc.6126.

Elfatih, A. & Eltahir, B. 1992 Drought frequency analysis of annual rainfall series in central and western Sudan. *Hydrological Sciences Journal* **37** (3), 185–199. https://doi.org/10.1080/02626669209492581.

Esaias, W. E., Abbott, M. R., Barton, I., Brown, O. B., Campbell, J. W., Carder, K. L., Clark, D. K., Evans, R. H., Hoge, F. E., Gordon, H. R., Balch, W. M., Letelier, R. & Minnett, P. J. 1998 An overview of MODIS capabilities for ocean science observations. *IEEE Transactions on Geoscience and Remote Sensing* **36** (4), 1250–1265. https://doi.org/10.1109/36.701076.

Ezzine, H., Bouziane, A. & Ouazar, D. 2014 Seasonal comparisons of meteorological and agricultural drought indices in Morocco using open short time-series data. *International Journal of Applied Earth Observation and Geoinformation* **26**, 36–48. https://doi.org/10.1016/j.jag.2013.05.005.

Fniguire, F., Laftouhi, N.-E., Saidi, M. E. & Markhi, A. 2014 Some aspects of climate variability and increasing aridity in central Morocco over the last forty years : Case of Tensift Basin (Marrakech-Morocco). *Journal of Environment and Earth Science* **4** (9), 42–51.

Fniguire, F., Laftouhi, N.-E., Saidi, M. E., Zamrane, Z., El Himer, H. & Khalil, N. 2017 Spatial and temporal analysis of the drought vulnerability and risks over eight decades in a semi-arid region (Tensift basin: Morocco). *Theoretical and Applied Climatology* **130** (1-2), 321–330. https://doi.org/10.1007/s00704-016-1873-z.

Fung, K. F., Huang, Y. F., Koo, C. H. & Soh, Y. W. 2019 Drought forecasting : A review of modelling approaches 2007–2017. *Journal of Water and Climate Change* **11** (3), 771–799. https://doi.org/10.2166/wcc.2019.236.

Gao, F., Wang, Y., Chen, X. & Yang, W. 2020 Trend analysis of rainfall time series in Shanxi Province, Northern China (1957–2019). *Water* **12** (9), Article 9. https://doi.org/10.3390/w12092335.

Gumus, V., Simsek, O., Avsaroglu, Y. & Agun, B. 2021 Spatio-temporal trend analysis of drought in the GAP Region, Turkey. *Natural Hazards* **109** (2), 1759–1776. https://doi.org/10.1007/s11069-021-04897-1.

Guttman, N. B. 1994 On the sensitivity of sample L moments to sample size. *Journal of Climate* **7** (6), 1026–1029.

Habibi, B. & Meddi, M. 2021 Meteorological drought hazard analysis of wheat production in the semi-arid basin of Cheliff–Zahrez Nord, Algeria. *Arabian Journal of Geosciences* **14** (11), 1045. https://doi.org/10.1007/s12517-021-07401-y.

Habitou, N., Morabbi, A., Ouazar, D., Bouziane, A., Hasnaoui, M. D. & Sabri, H. 2020 CHIRPS precipitation open data for drought monitoring : Application to the Tensift basin, Morocco. *Journal of Applied Remote Sensing* **14** (3), 034526. https://doi.org/10.1117/1.JRS.14.034526.

Hadri, A., Saidi, M. E. M. & Boudhar, A. 2021a Multiscale drought monitoring and comparison using remote sensing in a Mediterranean arid region: A case study from west-central Morocco. *Arabian Journal of Geosciences* **14** (2), 118. https://doi.org/10.1007/s12517-021-06493-w.

Hadri, A., Saidi, M. E. M., Saouabe, T. & El Alaoui El Fels, A. 2021b Temporal trends in extreme temperature and precipitation events in an arid area : Case of Chichaoua Mejjate region (Morocco). *Journal of Water and Climate Change* **12** (3), 895–915. https://doi.org/10.2166/wcc.2020.234.

Hadri, A., Saidi, M. E. M., El Khalki, E. M., Aachrine, B., Saouabe, T. & Elmaki, A. A. 2022 Integrated water management under climate change through the application of the WEAP model in a Mediterranean arid region. *Journal of Water and Climate Change* **13** (6), 2414–2442. https://doi.org/10.2166/wcc.2022.039.

Hadria, R., Boudhar, A., Ouatiki, H., Lebrini, Y., Elmansouri, L., Gadouali, F., Hayat Lionboui, H. L. & Benabdelouahab, T. 2019 Combining use of TRMM and ground observations of annual precipitations for meteorological drought trends monitoring in Morocco. *American Journal of Remote Sensing* **7** (2), 25. https://doi.org/10.11648/j.ajrs.20190702.11.

Hanadé Houmma, I., El Mansouri, L., Gadal, S., Mamane Barkawi, M. B. & Hadria, R. 2022 Prospective analysis of spatial heterogeneity influence on the concordance of remote sensing drought indices: A case of semi-arid agrosystems in Morocco (Moulouya and Tensift watersheds). *Geocarto International* **37** (27), 14899–14924. https://doi.org/10.1080/10106049.2022.2092219.

Heim, J. & Richard, R. 2002 A review of twentieth-century drought indices used in the United States. *Bulletin of the American Meteorological Society* **83** (8), 1149–1166. https://doi.org/10.1175/1520-0477-83.8.1149.

Herrmann, S. M., Didan, K., Barreto-Munoz, A. & Crimmins, M. A. 2016 Divergent responses of vegetation cover in Southwestern US ecosystems to dry and wet years at different elevations. *Environmental Research Letters* **11** (12), 124005. https://doi.org/10.1088/1748-9326/11/12/124005.

Hurrell, J. W., Kushnir, Y., Ottersen, G. & Visbeck, M. 2003 An overview of the North Atlantic Oscillation. *Geophysical Monograph Series* **134**, 1–35. https://doi.org/10.1029/134GM01.

Ikechukwu, M. N., Ebinne, E., Idorenyin, U. & Raphael, N. I. 2017 Accuracy assessment and comparative analysis of IDW, spline and kriging in spatial interpolation of landform (Topography): An experimental study. *Journal of Geographic Information System* **09** (03), 354–371. https://doi.org/10.4236/jgis.2017.93022.

Jamro, S., Channa, F. N., Dars, G. H., Ansari, K. & Krakauer, N. Y. 2020 Exploring the evolution of drought characteristics in Balochistan, Pakistan. *Applied Sciences* **10** (3), 913. https://doi.org/10.3390/app10030913.

Javed, T., Yao, N., Chen, X., Suon, S. & Li, Y. 2020 Drought evolution indicated by meteorological and remote-sensing drought indices under different land cover types in China. *Environmental Science and Pollution Research* **27** (4), 4258–4274. https://doi.org/10.1007/s11356-019-06629-2.

JICA, MATEE, & ABHT 2008 *Etude du plan de gestion intégrée des ressources en eau dans la plaine du Haouz : Royaume du Maroc (Rapport Final)*. Pacific Consultants International. Available from: http://www.abhatoo.net.ma/maalama-textuelle/developpement-durable/environnement/eau-douce/approvisionnement-en-eau-potable/traitement-de-l-eau/etude-du-plan-de-gestion-integree-des-ressources-en-eau-dans-la-plaine-du-haouz-royaume-du-maroc-rapport-final.

Junaid, M. 2021 Rainfall trend analysis by Mann-Kendall test and Sen's slope estimator: A case study of Gummidipoondi Sub-basin, Tamil Nadu, India. *International Journal of Scientific and Engineering Research* **12** (6), 575.

Justice, C. O., Vermote, E., Townshend, J. R. G., Defries, R., Roy, D. P., Hall, D. K., Salomonson, V. V., Privette, J. L., Riggs, G., Strahler, A., Lucht, W., Myneni, R. B., Knyazikhin, Y., Running, S. W., Nemani, R. R., Wan, Z., Huete, A. R., van Leeuwen, W., Wolfe, R. E., Giglio, L., Muller, J., Lewis, P. & Barnsley, M. J. 1998 The moderate resolution imaging spectroradiometer (MODIS) : Land remote sensing for global change research. *IEEE Transactions on Geoscience and Remote Sensing* **36** (4), 1228–1249. https://doi.org/10.1109/36.701075.

Khomsi, K., Mahe, G., Tramblay, Y., Sinan, M. & Snoussi, M. 2016 Regional impacts of global change: Seasonal trends in extreme rainfall, run-off and temperature in two contrasting regions of Morocco. *Natural Hazards and Earth System Sciences* **16** (5), 1079–1090. https://doi.org/10.5194/nhess-16-1079-2016.

Kim, J.-S., Park, S.-Y., Lee, J.-H., Chen, J., Chen, S. & Kim, T.-W. 2021 Integrated drought monitoring and evaluation through multi-sensor satellite-based statistical simulation. *Remote Sensing* **13** (2), Article 2. https://doi.org/10.3390/rs13020272.

King, M. D., Menzel, W. P., Kaufman, Y. J., Tanre, D., Gao, B.-C., Platnick, S., Ackerman, S. A., Remer, L. A., Pincus, R. & Hubanks, P. A. 2003 Cloud and aerosol properties, precipitable water, and profiles of temperature and water vapor from MODIS. *IEEE Transactions on Geoscience and Remote Sensing* **41** (2), 442–458. https://doi.org/10.1109/TGRS.2002.808226.

Knippertz, P., Ulbrich, U., Marques, F. & Corte-Real, J. 2003 Decadal changes in the link between El Niño and springtime North Atlantic oscillation and European–North African rainfall. *International Journal of Climatology* **23** (11), 1293–1311. https://doi.org/10.1002/joc.944.

Kogan, F. N. 1995 Application of vegetation index and brightness temperature for drought detection. *Advances in Space Research* **15** (11), 91–100. https://doi.org/10.1016/0273-1177(95)00079-T.

Kogan, F. N. 2000 Contribution of remote sensing to drought early warning. In: *Early Warning Systems for Drought Preparedness and Drought Management. Proceedings of an Expert Group Meeting Held*, Lisbon, Portugal.

Kulkarni, S. S., Wardlow, B. D., Bayissa, Y. A., Tadesse, T., Svoboda, M. D. & Gedam, S. S. 2020 Developing a remote sensing-based combined drought indicator approach for agricultural drought monitoring over Marathwada, India. *Remote Sensing* **12** (13), 2091. https://doi.org/10.3390/rs12132091.

Li, J., Zhou, S. & Hu, R. 2016 Hydrological drought class transition using SPI and SRI time series by loglinear regression. *Water Resources Management* **30** (2), 669–684. https://doi.org/10.1007/s11269-015-1184-7.

Liu, H., Chen, S., Hou, M. & He, L. 2020 Improved inverse distance weighting method application considering spatial autocorrelation in 3D geological modeling. *Earth Science Informatics* **13** (3), 619–632. https://doi.org/10.1007/s12145-019-00436-6.

Lkammarte, F. Z., Eddoughri, F., Karmaoui, A., Khebiza, M. Y. & Messouli, M. 2023 Analysis of the vulnerability of agriculture to climate and anthropogenic change in Marrakech Safi region, Morocco. *Applied Ecology and Environmental Research* **21** (1), 519–544. https://doi.org/10.15666/aeer/2101_519544.

Malik, A., Kumar, A., Pham, Q. B., Zhu, S., Linh, N. T. T. & Tri, D. Q. 2020 Identification of EDI trend using Mann-Kendall and Şen-innovative trend methods (Uttarakhand, India). *Arabian Journal of Geosciences* **13** (18), 951. https://doi.org/10.1007/s12517-020-05926-2.

McKee, T. B., Doesken, N. J. & Kleist, J. 1993 *The Relationship of Drought Frequency and Duration to Time Scales*. 6.

Mishra, A. K. & Singh, V. P. 2010 A review of drought concepts. *Journal of Hydrology* **391** (1–2), 202–216. https://doi.org/10.1016/j.jhydrol.2010.07.012.

Mounir, K., La Jeunesse, I., Sellami, H. & Elkhanchoufi, A. 2023 Spatiotemporal analysis of drought occurrence in the Ouergha catchment, Morocco. *AIMS Environmental Science* **10** (3), 398–423. https://doi.org/10.3934/environsci.2023023.

Najmi, A., Igmoullan, B., Namous, M., El Bouazzaoui, I., Brahim, Y. A., El Khalki, E. M. & Saidi, M. E. M. 2023 Evaluation of PERSIANN-CCS-CDR, ERA5, and SM2RAIN-ASCAT rainfall products for rainfall and drought assessment in a semi-arid watershed, Morocco. *Journal of Water and Climate Change* **14** (5), 1569–1584. https://doi.org/10.2166/wcc.2023.461.

Nalbantis, I. & Tsakiris, G. 2009 Assessment of hydrological drought revisited. *Water Resources Management* **23** (5), 881–897. https://doi.org/10.1007/s11269-008-9305-1.

Niazi, S. 2007 *Evaluation des impacts des changements climatiques et de l'élévation du niveau de la mer sur le littoral de Tétouan (Méditerranée occidentale du Maroc) : Vulnérabilité et Adaptation.* [Université Mohammed V- Agdal]. thesesenafrique.imist.ma.

Ouassanouan, Y., Fakir, Y., Simonneaux, V., Kharrou, M. H., Bouimouass, H., Najar, I., Benrhanem, M., Sguir, F. & Chehbouni, A. 2022 Multi-decadal analysis of water resources and agricultural change in a Mediterranean semiarid irrigated piedmont under water scarcity and human interaction. *Science of The Total Environment* **834**, 155328. https://doi.org/10.1016/j.scitotenv.2022.155328.

Ouatiki, H., Boudhar, A., Ouhinou, A., Arioua, A., Hssaisoune, M., Bouamri, H. & Benabdelouahab, T. 2019 Trend analysis of rainfall and drought over the Oum Er-Rbia River Basin in Morocco during 1970–2010. *Arabian Journal of Geosciences* **12** (4), 128. https://doi.org/10.1007/s12517-019-4300-9.

Ouatiki, H., Boudhar, A. & Chehbouni, A. 2023 Accuracy assessment and bias correction of remote sensing–based rainfall products over semiarid watersheds. *Theoretical and Applied Climatology* 1–18. https://doi.org/10.1007/s00704-023-04586-y.

Pathak, A. A. & Dodamani, B. M. 2020 Trend analysis of rainfall, rainy days and drought : A case study of Ghataprabha River Basin, India. *Modeling Earth Systems and Environment* **6** (3), 1357–1372. https://doi.org/10.1007/s40808-020-00798-7.

Salomonson, V. V., Barnes, W., Xiong, J., Kempler, S. & Masuoka, E. 2002 An overview of the earth observing system MODIS instrument and associated data systems performance. *IEEE International Geoscience and Remote Sensing Symposium* **2**, 1174–1176. https://doi.org/10.1109/IGARSS.2002.1025812.

Saouabe, T., Naceur, K. A., El Khalki, E. M., Hadri, A. & Saidi, M. E. 2022 GPM-IMERG product: A new way to assess the climate change impact on water resources in a Moroccan semi-arid basin. *Journal of Water and Climate Change* **13** (7), 2559–2576. https://doi.org/10.2166/wcc.2022.403.

Seiler, R. A., Kogan, F. & Sullivan, J. 1998 AVHRR-based vegetation and temperature condition indices for drought detection in Argentina. *Advances in Space Research* **21** (3), 481–484. https://doi.org/10.1016/S0273-1177(97)00884-3.

Senamaw, A., Addisu, S. & Suryabhagavan, K. V. 2021 Mapping the spatial and temporal variation of agricultural and meteorological drought using geospatial techniques, Ethiopia. *Environmental Systems Research* **10** (1), 15. https://doi.org/10.1186/s40068-020-00204-2.

Sun, J., Xiong, X., Guenther, B. W. & Barnes, W. 2003 Radiometric stability monitoring of the MODIS reflective solar bands using the Moon. *Metrologia* **40** (1), S85–S88. https://doi.org/10.1088/0026-1394/40/1/319.

Tsakiris, G. & Vangelis, H. 2004 Towards a drought watch system based on spatial SPI. *Water Resources Management* **18** (1), 1–12. https://doi.org/10.1023/B:WARM.0000015410.47014.a4.

USGS 2021 *Earth Explorer* [Plateforme]. USGS Science for a Changing World. Available from: https://earthexplorer.usgs.gov/.

Vicente-Serrano, S. M., Beguería, S. & López-Moreno, J. I. 2010 A multiscalar drought index sensitive to global warming: The standardized precipitation evapotranspiration index. *Journal of Climate* **23** (7), 1696–1718. https://doi.org/10.1175/2009JCLI2909.1.

Vicente-Serrano, S. M., López-Moreno, J. I., Lorenzo-Lacruz, J., Kenawy, A. E., Azorin-Molina, C., Morán-Tejeda, E., Pasho, E., Zabalza, J., Beguería, S. & Angulo-Martínez, M. 2011 The NAO impact on droughts in the mediterranean region. In: *Hydrological, Socioeconomic and Ecological Impacts of the North Atlantic Oscillation in the Mediterranean Region* (Vicente-Serrano, S. M. & Trigo, R. M., eds). Springer, Netherlands. https://doi.org/10.1007/978-94-007-1372-7_3.

Wan, Z. 2013 *MODIS Land Surface Temperature Products users' guide* (805; p. 33). Institute for Computational Earth System Science. Available from: https://lpdaac.usgs.gov/documents/447/MOD11_User_Guide_V4.pdf.

Wang, H., Lin, H. & Liu, D. 2014 Remotely sensed drought index and its responses to meteorological drought in Southwest China. *Remote Sensing Letters* **5** (5), 413–422. https://doi.org/10.1080/2150704X.2014.912768.

Wang, Q., Shi, P., Lei, T., Geng, G., Liu, J., Mo, X., Li, X., Zhou, H. & Wu, J. 2015 The alleviating trend of drought in the Huang-Huai-Hai Plain of China based on the daily SPEI : The alleviating trend of drought in the Huang-Huai-Hai plain of China. *International Journal of Climatology* **35** (13), 3760–3769. https://doi.org/10.1002/joc.4244.

Wang, X., Jiang, D. & Lang, X. 2018 Climate change of 4 °C global warming above pre-industrial levels. *Advances in Atmospheric Sciences* **35** (7), 757–770. https://doi.org/10.1007/s00376-018-7160-4.

Wilhite, D. 2000 Drought as a Natural Hazard : Concepts and Definitions. In Drought Mitigation Center Faculty Publications (A Global Assessment, Vol. 1, p. 3–18). Available from: https://digitalcommons.unl.edu/droughtfacpub/69.

World Bank 2013 *Climate-Induced Spatio-Temporal Shifts in Natural and Agro-Ecosystems in the Middle East and North Africa Region [Synthesis Report]*. https://doi.org/10.1596/35368. World Bank, Washington, DC, USA.

Wyss, D., Negussie, K., Staacke, A., Karnagel, A., Engelhardt, M. & Kappas, M. 2022 A comparative analysis of MODIS-derived drought indices for Northern and Central Namibia. *African Journal of Environmental Science and Technology* **16** (5), 173–191. https://doi.org/10.5897/AJEST2022.3096.

Xiong, X. & Barnes, W. 2006 An overview of MODIS radiometric calibration and characterization. *Advances in Atmospheric Sciences* **23** (1), 69–79. https://doi.org/10.1007/s00376-006-0008-3.

Xiong, X., Che, N. & Barnes, W. 2005 Terra MODIS on-orbit spatial characterization and performance. *IEEE Transactions on Geoscience and Remote Sensing* **43** (2), 355–365. https://doi.org/10.1109/TGRS.2004.840643.

Yue, S. & Pilon, P. 2004 A comparison of the power of the t test, Mann-Kendall and bootstrap tests for trend detection/Une comparaison de la puissance des tests t de Student, de Mann-Kendall et du bootstrap pour la détection de tendance. *Hydrological Sciences Journal* **49** (1), 21–37. https://doi.org/10.1623/hysj.49.1.21.53996.

Zeng, J., Zhang, R., Qu, Y., Bento, V. A., Zhou, T., Lin, Y., Wu, X., Qi, J., Shui, W. & Wang, Q. 2022 Improving the drought monitoring capability of VHI at the global scale via ensemble indices for various vegetation types from 2001 to 2018. *Weather and Climate Extremes* **35**, 100412. https://doi.org/10.1016/j.wace.2022.100412.

Zkhiri, W., Tramblay, Y., Hanich, L., Jarlan, L. & Ruelland, D. 2018 Spatiotemporal characterization of current and future droughts in the High Atlas basins (Morocco). *Theoretical and Applied Climatology* **135** (1-2), 593–605. https://doi.org/10.1007/s00704-018-2388-6.

First received 22 June 2023; accepted in revised form 16 October 2023. Available online 27 October 2023